


---

# Barcode activity in a recurrent network model of the hippocampus enables efficient memory binding

---


Ching Fang<sup>1\*</sup>, Jack Lindsey<sup>2\*</sup>, L.F. Abbott<sup>1</sup>, Dmitry Aronov<sup>1,3</sup>, and Selmaan Chettih<sup>1</sup> 

<sup>1</sup>Zuckerman Mind Brain Behavior Institute, Columbia University

<sup>2</sup>Anthropic (work conducted while at Columbia University)

<sup>3</sup>Howard Hughes Medical Institute at Columbia University

\*equal contribution

 corresponding author: [sc4551@columbia.edu](mailto:sc4551@columbia.edu)

## Abstract

Forming an episodic memory requires binding together disparate elements that co-occur in a single experience. One model of this process is that neurons representing different components of a memory bind to an "index" — a subset of neurons unique to that memory. Evidence for this model has recently been found in chickadees, which use hippocampal memory to store and recall locations of cached food. Chickadee hippocampus produces sparse, high-dimensional patterns ("barcodes") that uniquely specify each caching event. Unexpectedly, the same neurons that participate in barcodes also exhibit conventional place tuning. It is unknown how barcode activity is generated, and what role it plays in memory formation and retrieval. It is also unclear how a memory index (e.g. barcodes) could function in the same neural population that represents memory content (e.g. place). Here, we design a biologically plausible model that generates barcodes and uses them to bind experiential content. Our model generates barcodes from place inputs through the chaotic dynamics of a recurrent neural network and uses Hebbian plasticity to store barcodes as attractor states. The model matches experimental observations that memory indices (barcodes) and content signals (place tuning) are randomly intermixed in the activity of single neurons. We demonstrate that barcodes reduce memory interference between correlated experiences. We also show that place tuning plays a complementary role to barcodes, enabling flexible, contextually-appropriate memory retrieval. Finally, our model is compatible with previous models of the hippocampus as generating a predictive map. Distinct predictive and indexing functions of the network are achieved via an adjustment of global recurrent gain. Our results suggest how the hippocampus may use barcodes to resolve fundamental tensions between memory specificity (pattern separation) and flexible recall (pattern completion) in general memory systems.

## 1 Introduction

Humans and other animals draw upon memories to shape their behaviors in the world. Memories of specific personal experiences — called episodic memories (Tulving et al., 1972) — are particularly important for livelihood. In animals, episodic-like memory is operationally defined as the binding of the “where”, “what”, and “when” components that comprise a single experience. This information can later be retrieved from memory to affect behavior flexibly, depending on context (Clayton and Dickinson, 1998). The binding of memory contents into a discrete memory is thought to occur in hippocampus. Previous work proposed that hippocampus supports memory by generating an “index”, that is, a signal distinct from the contents of a memory (Teyler and DiScenna, 1986; Teyler and Rudy, 2007). In this scheme, during

9 memory formation, plasticity links the neurons that represent memory contents with the neurons that generate this  
10 index. Later reactivation of the index drives recall of the memory contents.

11 Indexing theory was originally articulated at an abstract level, without reference to particular neural repre-  
12 sentations (Teyler and DiScenna, 1986). More recently, signatures of index signals were identified in neural activity  
13 through experiments in food-caching chickadees (*Poecile atricapillus*), an influential animal model of episodic memory  
14 (Sherry, 1984). Chettih et al. (2024) identified “barcode”-like activity in the chickadee hippocampus during memory  
15 formation and suggested that barcodes function as memory indices. Barcodes are sparse, high-dimensional patterns of  
16 hippocampal activity that occur transiently during caching. They are unique to each cache and are uncorrelated between  
17 cache sites, even for nearby sites with similar place tuning. Barcodes are then reactivated when a bird retrieves the  
18 cached item. Chickadee hippocampus also encodes the bird’s location — as expected, given the presence of place cells  
19 — as well as the presence of a cached sunflower seed, irrespective of location. Thus, Chettih et al. (2024) found that  
20 hippocampal activity contains both putative memory indices (in the form of barcodes) and putative memory content (in  
21 the form of place and seed-related activity).

22 These findings raise several critical questions. How are barcodes generated and associated with place and  
23 seed-related activity during caching? How can hippocampal dynamics subsequently recall these same patterns during  
24 retrieval? Critically, neurons participate in both barcodes and place codes with near random overlap, in contrast with  
25 theoretical models where content and indexing functions occur in separate neurons (Krotov and Hopfield, 2016; Bricken  
26 and Pehlevan, 2021; Tyulmankov et al., 2021; Whittington et al., 2021; Kozachkov et al., 2023). It is unclear at a  
27 computational level how memory index and content signals can be functionally distinct when they coexist in the same  
28 network and even in the activities of single neurons.

29 In this paper, we use the findings of Chettih et al. (2024) to guide the design of a biologically-plausible  
30 recurrent neural network (RNN) for cache memory formation and recall. The model generates barcodes and associates  
31 them with memory content in the same neural population. At recall time, the model can flexibly adjust the spatial scale  
32 of its memory retrieval, ranging from site-specific information to search of an extended area, depending on contextual  
33 demands. Using this model, we demonstrate the computational advantages of barcode-mediated memory by showing  
34 that it reduces interference between similar memories. We also show that place and barcode activities in the model play  
35 complementary roles in enabling memory specificity and flexible recall.

## 36 **2 Results**

### 37 **2.1 Barcode representations in the hippocampus are observed during caching**

38 We first review the key experimental results in Chettih et al. (2024). Black-capped chickadees were placed in a  
39 laboratory arena comprised of a grid of identical sites. Each site had a perch to land on and a hidden compartment,  
40 covered by a flap, where a seed could be hidden. Chickadees were allowed to behave freely in this environment and

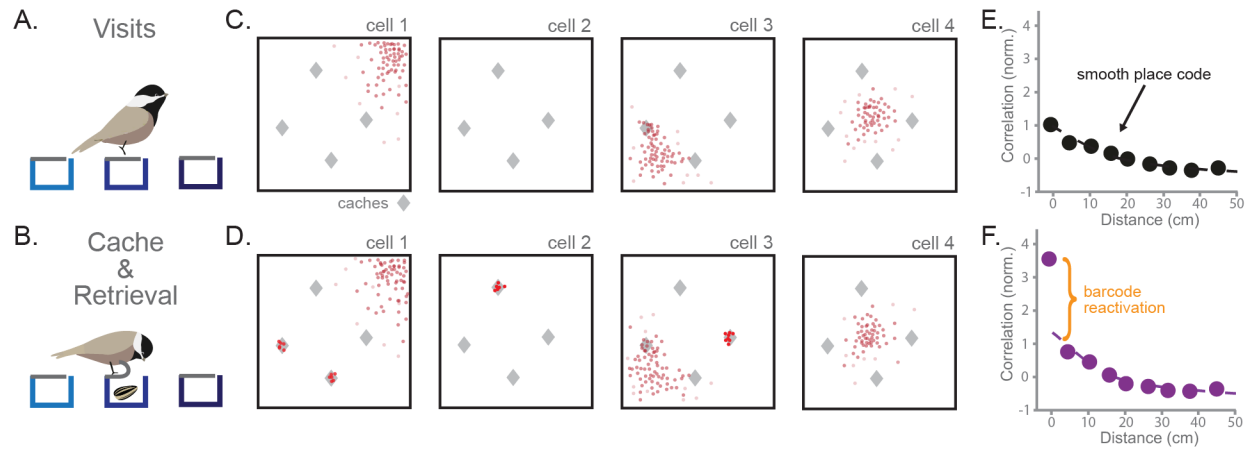


**Figure 1: Hippocampal activity during food-caching reveals sparse “barcodes” for each cache memory.** **A.** A black-capped chickadee visits cache sites in a laboratory arena. The chickadee does not interact with cache sites during what we call a visit. **B.** A chickadee caches or retrieves at a cache site by peeling back the rubber flap at the site. This reveals a hidden compartment where seeds can be stored. **C.** Cartoon example of spiking activity during visits of four hippocampal neurons in a square arena. Spikes are in red. Gray diamonds indicate the location of sites with caches. **D.** As in (C), for the same cells during caching and retrieval. Neurons fire sparsely and randomly during caches (activity clusters at sites) independent of their place tuning. **E.** Correlation of population activity during visits to the same or different sites of increasing distance. Values are max-normalized. Reproduced with permission from [Chettih et al. \(2024\)](#). **F.** As in (E), but comparing activity from caches at a site to activity from retrievals at the same or different sites. Barcode activity shared between caches and retrievals at the same site produces a sharp deviation from smooth spatial tuning. Values are normalized by the same factor as in (E). Reproduced with permission from [Chettih et al. \(2024\)](#).

41 collect sunflower seeds from feeders. A chickadee often visited sites without interacting with the hidden compartment  
42 (Figure 1A) but, at other times, the chickadee cached a seed into the compartment, or retrieved a previously cached  
43 seed (Figure 1B). Previous experiments demonstrated that chickadees remember the precise sites of their caches in this  
44 behavioral paradigm ([Applegate and Aronov, 2022](#)).

45 [Chettih et al. \(2024\)](#) recorded hippocampal population activity during these behaviors. When chickadees  
46 visited sites, place cells were observed, similar to those previously found in birds and mammals ([Payne et al., 2021](#))  
47 (Figure 1C). Place cells did not change their spatial tuning after a cache. Instead, during caching and retrieval, neurons  
48 transiently displayed memory-related activity. During caching, neurons fired sparsely, with individual neurons producing  
49 large activity bursts for a small subset of caches at seemingly random locations (Figure 1D). These bursts occurred  
50 in both place cells and non-place cells, with the location of cache bursts unrelated to a neuron’s place tuning. At  
51 the population level, activity during a cache consisted of both typical place activity and a cache-specific component  
52 orthogonal to the place code, termed a “barcode”. Strikingly, barcode activity for a particular cache reactivated during  
53 later retrieval of that cache. These findings were evident when examining the correlation between population activity  
54 vectors for visits, caches and retrievals at different sites. When comparing two visits, the correlation profile decayed  
55 smoothly with distance, as expected from place tuning (Figure 1E). When comparing caching with retrieval, a similar  
56 smooth decay was observed for most distances, indicating the presence of place tuning. However, there was a substantial  
57 boost in correlation for caches and retrievals at the exact same site (Figure 1F). This site-specific boost resulted from  
58 reactivation of the cache barcode during subsequent retrieval.

Barcode activity during caching and retrieval, which are moments of memory formation and recall, suggests a mechanism supporting episodic memory. We hypothesize that the hippocampus generates a sparse, high-dimensional pattern of activity transiently during the formation of each memory, and that this serves as a unique index to which the contents of the memory are bound. Reactivation of the barcode at a later time drives the recall of the associated memory contents. In the food caching behavior studied by Chettih et al. (2024), the contents of memory include the location (“where”) and presence of a seed (“what”). Below, we implement this hypothesis in a computational model.

## 2.2 Generating barcode activity with random recurrent dynamics.

We model the hippocampus as a recurrent neural network (RNN) (Alvarez and Squire, 1994; Tsodyks, 1999; Hopfield, 1982) and propose that recurrent dynamics can generate barcodes from place inputs (Figure 2A). Place inputs into the network are termed  $\vec{p}$ , and are spatially correlated as follows. Each neuron in the RNN receives inputs that are maximal at one location in the environment and decay with distance from that location, causing the neuron to have a single place field centered at that location. Across neurons, place fields uniformly span the environment. The firing rate activity of RNN units is denoted as  $\vec{x}$ . The recurrent weights of the model are given by  $J$ , and the RNN activity  $\vec{x}$  follows standard dynamics equations:

$$\vec{x} = \text{ReLU}(\vec{v}) \quad (1)$$

$$\frac{d\vec{v}}{dt} = -g(\vec{x})\vec{v} + J\vec{x} + \vec{p} \quad (2)$$

where  $\vec{v}$  is the voltage signal of the RNN units and  $g(\cdot)$  is a leak rate that depends on the average activity of the full network, representing a form of global shunting inhibition that controls overall network activity. In our simulations, we simplify the task by using a 1D circular environment binned into 100 discrete spatial “states”. We set the spatial correlation length scale of place inputs such that the smallest distance between cache sites in the experiments of Chettih et al. (2024) is equal to 8 of these states (see Methods for more details).

We initialize the recurrent weights from a random Gaussian distribution ( $J \sim \mathcal{N}(\frac{\mu}{N_x}, \frac{\sigma^2}{N_x})$ , where  $\mu < 0$ , reflecting global subtractive inhibition, and  $N_x$  is the number of RNN neurons). We first consider network activity before any learning-related changes. For the range of parameters we use, the network is in a chaotic state with a roughly constant overall level of activity but fluctuations in the activities of individual units. From an initial state of 0, we run recurrent dynamics until this steady-state level of overall activity has been achieved (Figure S1A,B). The chaotic recurrent dynamics induced by the random weights (Sompolinsky et al., 1988) effectively scrambles incoming place inputs. We demonstrate this by measuring the correlation of RNN activity across different locations and plotting this correlation as a function of distance (Figure 2B). Place inputs show a smoothly decaying correlation curve. At low values of  $\sigma$ , the network is primarily input driven, showing a smoothly decaying correlation matching inputs. At high values of  $\sigma$ , recurrence is so strong that it entirely eliminates the spatial correlation of nearby sites: activity at each state is decorrelated from activity at all other states.

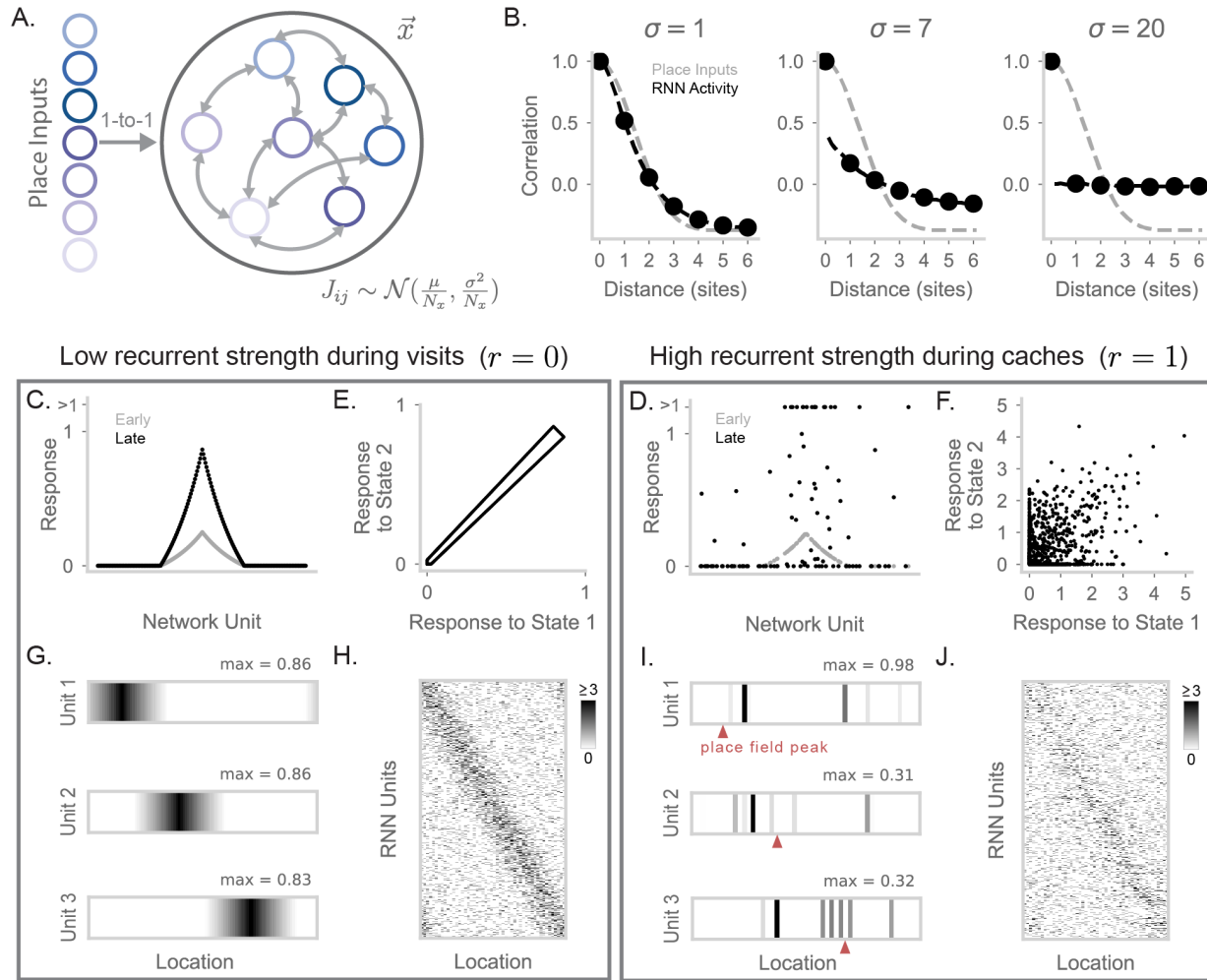


**Figure 2: A recurrent neural network generates barcode activity through recurrent dynamics.** **A.** Diagram of a recurrent neural network (RNN); the activity of the network units is denoted as  $\vec{x}$ . Place information arrives from an input layer with activities  $\vec{p}$ . Recurrent weights are initialized randomly, that is,  $J_{ij} \sim \mathcal{N}(\frac{\mu}{N_x}, \frac{\sigma^2}{N_x})$  for the synapse connecting neuron  $j$  to neuron  $i$ , where  $N_x$  is the number of RNN neurons. **B.** Correlation of activity vectors across different locations, when RNN weights are initialized with  $\sigma = 1$  (left),  $\sigma = 7$  (center), and  $\sigma = 20$  (right). We show correlation of place inputs (gray) and correlation of RNN activity (black) as  $\sigma$  is varied. X-axis is in units of site distance (see Methods for definition). **C.** Response of RNN units when simulating a visit to a location halfway around the circular track (with  $r = 0$ ; equation 3). In gray is the activity of the RNN at  $t = 0$ . In black is the activity at  $t = 100$ . 200 RNN units are uniformly subsampled and sorted by the tuning of their inputs for plotting purposes. **D.** As in (C), but for  $r = 1$ . RNN activity is more sparsely distributed, including high activity in neurons without place tuning for the current location. For visualization purposes, 50 RNN units with nonzero activity and 50 RNN units with 0 activity are sampled at this time point ( $t = 100$ ) for display, and responses greater than 1 are clipped to  $> 1$ . **E.** RNN activity in response to state 1 compared to state 2, when  $r = 0$ . Each point corresponds to a single RNN unit. **F.** As in (E), but for  $r = 1$ . RNN activity for these neighboring states is substantially decorrelated by recurrence. **G.** Firing fields of three example units on the circular track displaying place-cell activity. Maximum value of each field is labeled and the colormap is max-normalized. **H.** Simulated spike counts of a RNN population during visits to each location on the circular track. Spikes are generated by simulating Poisson-distributed counts from underlying unit rates. Place tuning results in a strong diagonal structure when units are sorted by their input's preferred location. The maximum limit of the colormap is set to the 99th percentile value of spike counts ( $\geq 3$  spikes). **I.** Same neurons as (G), but for  $r = 1$  with units now showing barcode activity. The location of the  $r = 0$  place field peak of each unit (i.e., its corresponding peak in (G)) is marked by a red triangle. **J.** As in (H), but for  $r = 1$ . The independence of barcode activity for neighboring sites results in a matrix with reduced diagonal structure.

90 Interestingly, at an intermediate level of  $\sigma = 7$ , the network retains elements from both high and low recurrence  
91 regimes (Figure 2B). The network exhibits a smoothly decaying correlation curve reflecting its inputs, but each state's  
92 activity also contains a strong decorrelated component, apparent in the large drop in correlations for nearby but non-  
93 identical sites. This intermediate network regime closely resembles spatial correlation profiles observed during caching  
94 (Chettih et al., 2024) (Figure 1F). The smoothly decaying component is caused by the place code, whereas the sharp  
95 peak at zero distance – reflecting barcode activity – is caused by the recurrent dynamics. We thus construct networks  
96 using intermediate  $\sigma$  values, which allow for the coexistence of place code and barcode components in population  
97 activity.

98 A key result from Chettih et al. (2024) is that the hippocampus exhibits both place code and barcode activity  
99 during caching and retrieval, but only place activity during visits. We propose that this effect can result from a network  
100 in which recurrent strength is flexibly modulated. In a low-recurrence condition, the network produces the place code,  
101 whereas in a high-recurrence condition the same network produces a combination of place code and barcode activity.  
102 To simulate this in our model, we modify equation 2 to

$$\frac{d\vec{v}}{dt} = -g(\vec{x})\vec{v} + rJ\vec{x} + \vec{p} \quad (3)$$

103 where the newly included  $r \in \{0, 1\}$  scales recurrent strength such that the network may be in a feedforward ( $r = 0$ ) or  
104 recurrent regime ( $r = 1$ ). During visits, we assume the network is operating with low recurrent strength ( $r = 0$ ). As a  
105 result, the activity in the RNN exhibits the spatial profile of its place inputs. We verify this is the case by visualizing  
106 early and late RNN activity given a place input (Figure 2C). With low recurrence, early and late RNN activity have  
107 similar spatial profiles, and late activity patterns for nearby states are highly correlated (Figure 2E). In contrast, when  
108 recurrence is enabled ( $r = 1$ ), network activity is sparse with a heavy tail of a few strongly active neurons, and is  
109 decorrelated between nearby states (Figure 2D,F). These changes match experimental observations of excitatory neurons  
110 during food caching (Chettih et al., 2024).

111 We visualized neural activity during visits ( $r = 0$ ) and caches ( $r = 1$ ). During visits, RNN units display  
112 ordinary place tuning (Figure 2G, S1C). We also simulated spikes for all units at each location, and visualized this  
113 as a matrix where units were sorted by the preferred location of their inputs (Figure 2H). This matrix exhibits a  
114 diagonal structure reflecting strong spatial correlations. During caches, single neurons develop sparse, scrambled spatial  
115 responses relative to their place tuning (Figure 2I, S1C). Accordingly, simulated spikes across the population have  
116 greater random, off-diagonal components during caching than during visits. Thus, recurrence in a randomly connected  
117 RNN is a simple and effective mechanism to generate barcode signals from spatially correlated inputs. We alternatively  
118 considered a feedforward mechanism to generate barcodes, in which barcodes are computed by a separate feedforward  
119 pathway (Figure S2). We found the feedforward mechanism required an unreasonably large number of neurons and  
120 sparsity levels to match the decorrelation level of the recurrent mechanism.



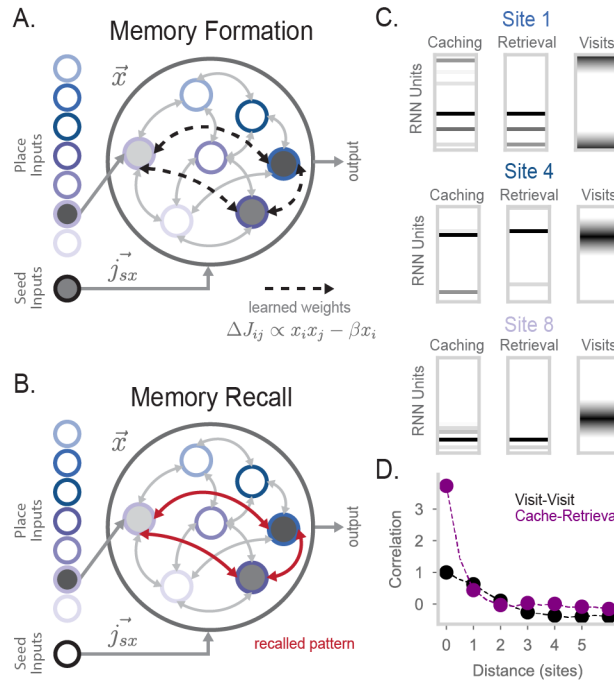


Figure 3: **Barcode activity binds content to store memories in the RNN.** **A.** Diagram of RNN activity during memory formation. Along with place inputs, a scalar seed input  $s$  is provided to the model.  $s$  connects to RNN units via 5000-dimensional weight vector  $j_{sx} \sim \mathcal{N}(0, 1)$ . During memory formation (i.e., when an animal caches a seed), place inputs representing the animal’s current location and a seed input are provided to the RNN. After recurrent dynamics are run for some time ( $t = 100$ ), the network undergoes Hebbian learning. **B.** An example of memory recall in the network. The animal is at the same location as in (A). The place input encoding that location is provided to the model and results in the RNN recalling the stored attractor pattern seen in (A). **C.** Examples of RNN population activity during caching (left), retrieval (center), and visits (right) at three sites. During visits the RNN has  $r = 0$ , while during caches and retrievals  $r = 1$ . For visualization purposes, 50 units are randomly sampled and displayed in the “Caching” and the “Retrieval” plot. **D.** Correlation of RNN activity at two sites, plotted as a function of the distance between the two sites. In black is the correlation in activity between two visits. In purple is the correlation between caching and retrieval activity. Experiments were simulated with 20 simulations where 5 sites were randomly chosen for caching. 99% confidence intervals are calculated over the simulations and plotted over the markers. Compare to Figure 1E,F.

### 121 2.3 Storing memories by binding content inputs with a barcode.

122 Having suggested a mechanism for the generation of barcode representations, we next propose how such a representation  
 123 can be leveraged for memory storage in a network model. In our food-caching task, we assume that the contents of a  
 124 memory include the location of the cache and the identity of a food item within the cache. Thus, we add an additional  
 125 input source besides spatial location into our model – an input  $s$  representing the presence of a seed (Figure 3A). The  
 126 “seed” input projects randomly onto the RNN neurons. During caching, both place inputs and seed inputs arrive into  
 127 the RNN, matching experimental findings (Chettih et al., 2024). This causes a mixed response in the network: one  
 128 component of the response (place activity) is spatially tuned, another component (seed activity) indicates the presence  
 129 of a seed and does not vary with location, and the third component (barcode activity) is generated by recurrent dynamics  
 130 interacting with these inputs.

131 To store memories, we assume the RNN undergoes Hebbian learning after some fixed time point during the  
132  $r = 1$  recurrent dynamics (Figure 3A). At this time, the synapse  $j \rightarrow i$  changes by an amount

$$\Delta J_{ij} \propto x_i x_j - \beta x_i \quad (4)$$

133 where  $\beta > 0$  provides an overall inhibition of the stored pattern. This term helps to prevent network activity from  
134 collapsing to previously stored attractors. Memory storage works as follows, following the experimentally observed  
135 sequence in Chettih et al. (2024): place inputs arrive into the RNN, recurrent dynamics form a barcode representation,  
136 seed inputs are activated, and then Hebbian learning binds a particular pattern of barcode activity to place- and seed-  
137 related activity. In this way, fixed-point attractors are formed corresponding to a conjunction of a barcode and memory  
138 content.

139 Memory recall in our network follows typical pattern completion dynamics, with recurrence strength set to  
140  $r = 1$  as for caches. As an example, consider a scenario in which an animal has already formed a memory at some  
141 location  $l$ , resulting in the storage of an attractor  $\vec{b}$  into the RNN. Later, the animal returns to the same location and  
142 attempts recall (i.e. sets  $r = 1$ , Figure 3B). The RNN receives inputs representing location  $l$ , which are partially  
143 correlated with  $\vec{b}$ , and recurrent attractor dynamics cause network activity to converge onto  $\vec{b}$ . This results in a  
144 reactivation of barcode activity, along with the place and seed components stored in the attractor state. The seed input  
145 can also affect recall, as discussed in the following section.

146 As an initial test of memory function in our model, we analyzed the activity patterns that are stored and  
147 recalled in the model. We simulated caching at different sites in the arena and extracted the population activity that is  
148 stored via Hebbian learning (Figure 3C, left). We then simulated retrieval as an event in which the animal returns to the  
149 same site and runs memory recall dynamics ( $r = 1$ ) in the RNN. Population activity during retrieval closely matches  
150 activity during caching, and is substantially decorrelated from activity during visits (Figure 3C). We find that population  
151 activity in the RNN is more strongly correlated between caches and retrievals at the same site than two visits to a site  
152 that are not seed related ( $r = 0$ ; Figure 3D). In addition, cache-retrieval correlations for non-identical sites rapidly drop  
153 to the level of visit-visit correlations because barcodes are orthogonal even for nearby sites. These correlation profiles  
154 closely resemble those observed in Chettih et al. (2024) (compare Figures 3D and 1E,F).

## 155 2.4 Barcode-mediated memory supports precise and flexible context-based memory recall

156 What are the computational benefits of barcode-mediated memory storage? We designed two behavioral tasks for our  
157 model that quantify complementary aspects of memory performance. In both tasks, we simulate a sequence of three  
158 caches in the circular arena. We then test the model's performance during memory recall (i.e.  $r = 1$ ) using two distinct  
159 tasks. The "Cache Presence" task requires the network to identify the presence or absence of a cached seed at the current  
160 location (Figure 4A). By evaluating the model on this task using different spacings between caches, we can measure the  
161 spatial precision of memory, i.e. how far apart two caches must be to prevent interference between their associated



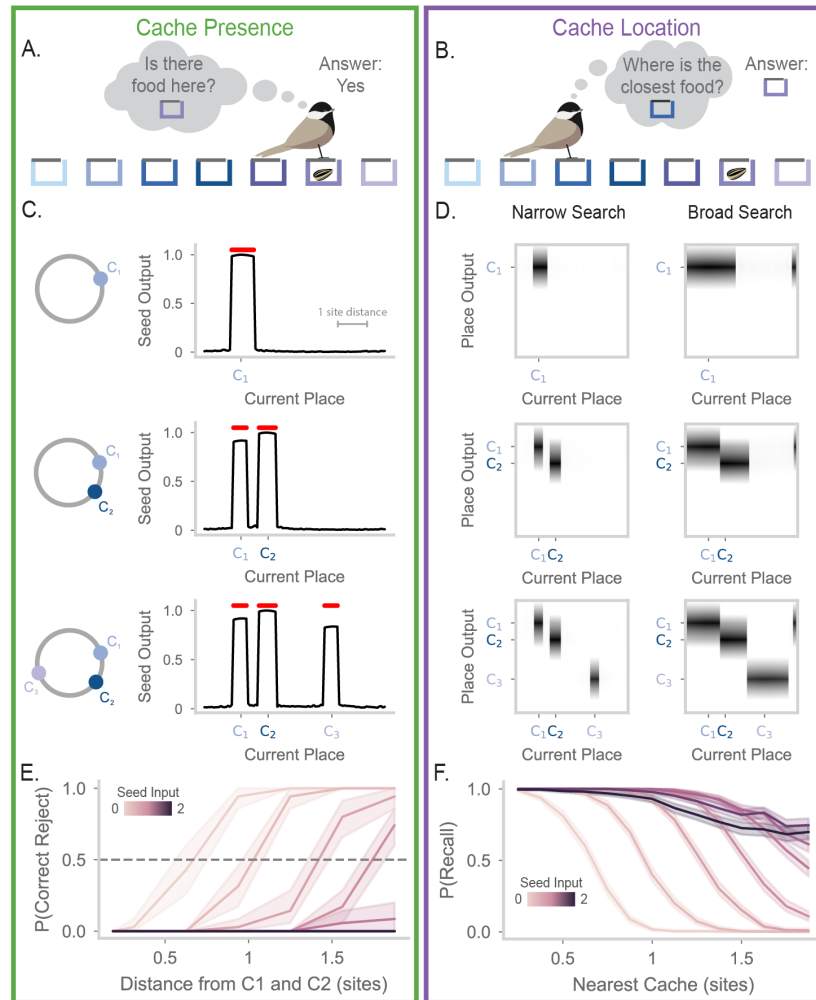


**Figure 4: Precise and flexible recall of barcode-mediated cache memories** **A.** Cartoon of a chickadee at a site, trying to remember whether the site contains a seed. The chickadee cannot see inside the hidden compartment and must rely on memory to answer this question. **B.** Cartoon of a chickadee at a site, trying to recall the location of the closest cache. In this case, the animal must use its memory to recall the location of a cache three sites away. **C.** Seed output of the RNN at different locations along the circular track. Red dots above the line indicate locations where the value is greater than 0.5. Top, results after the first cache is made at a location 20% of the way through the track. The location of the first cache is marked on the x-axis as  $C_1$ . Middle, same but after the second cache ( $C_2$ ) is made at a location 35% of the way through the track. Bottom, same but after the third cache ( $C_3$ ) is made at a location 70% of the way through the track. **D.** The place output of the RNN at different locations along the track. In the heatmaps, each column shows the activities of all the output units when the animal is at a particular location (horizontal axis). The left side panels of the subfigure correspond to the model operating at low recall strength ( $s = 0$ ). The right side panels correspond to the model operating at high recall strength ( $s = 1.5$ ). As in (C), top, middle, and bottom plots correspond to RNN activity after caches are made at  $C_1$ ,  $C_2$ , and  $C_3$ . Place output correctly switches between the location of each cache depending on proximity to the current position. **E.** Probability of correct reject rate in the model when the animal is at a location between caches 1 and 2, after all caches have been made. X-axis shows the distance from the probed location to the surrounding caches, measured in site distance. The color of each line corresponds to the recall strength  $s$ . At low recall strengths, the model correctly identified the absence of a cache between  $C_1$  and  $C_2$ , reflecting discrimination of the two cache locations. **F.** Probability of recalling the location of the closest cache, given the distance of the animal from the cache. A recall is considered successful if the seed output exceeds 0.5 and if the peak of the output corresponds to the location of the nearest cache. Lines are colored by recall strength  $s$ . The model correctly recalls the locations of nearby caches, with search radius increasing as recall strength increases.

162 memories. The “Cache Location” task requires the network to identify the cache nearest to the current location by  
163 reactivating place activity corresponding to that cache location (Figure 4B). This task measures the robustness of  
164 recall and requires attractor dynamics to accurately retrieve memories from potentially distant locations. Together,  
165 these questions probe the ability of the memory system to be both specific (pattern separation) and searchable (pattern  
166 completion).

167 To enable readout from the model, we add an output layer containing place and seed units. During memory  
168 formation, these units receive a copy of place and seed inputs, respectively, and undergo Hebbian plasticity (equation 4  
169 with  $\beta = 0$ ) with RNN units. This enables the RNN to reactivate a copy of the inputs that were provided during memory  
170 formation. We measure the activity of the seed output to determine cache presence, and we measure place outputs to  
171 determine cache location. We note that other readout mechanisms would likely function similarly – for example, plastic  
172 feedback connectivity from recurrent onto inputs units. The output layer used here is not intended to correspond to  
173 a specific brain region, but simply to provide a window into what could be read out easily from network activity by  
174 downstream neural circuits.

175 We first show model performance on a single example of the Cache Presence and Cache Location tasks, where  
176 caches are made at the locations 20%, 35%, and 70% of the way around the circular track. For the Cache Presence  
177 task, we evaluate the model at each spatial location and plot the activity of the seed output (Figure 4C). After the first  
178 cache, we see that the seed output is only high at states around the vicinity of the first cache (Figure 4C, top). The false  
179 positive rate is not zero since the states around the cache also have high output. However, the width of this false positive  
180 area is less than the distance between two sites in the arena used in [Chettih et al. \(2024\)](#), indicating that the model is  
181 able to identify caches at the spatial resolution observed in chickadee behavior in these experiments. After a second  
182 cache, the seed output correctly reports seeds in the areas around the two caches (Figure 4C, middle). Importantly, the  
183 network separates the caches from each other, correctly identifying the absence of a seed at a position between the two  
184 caches. This behavior is maintained after the addition of the final third cache (Figure 4C, bottom).

185 For the Cache Location task, we examine the place outputs (Figure 4D, “Narrow Search”). When the current  
186 position is near a cache, the network correctly outputs a place field for the location of the nearest cache. However, an  
187 animal relying on memory to guide behavior may need to recall cache locations even when far away from a cache. To  
188 enable increased search radius, we make use of the seed input, which can bias network activity towards all memory  
189 patterns previously associated with this input. Activating the seed input greatly increases the range of current positions  
190 over which cache memories are retrieved (Figure 4D, “Broad Search”). Critically, this does not cause interference  
191 between memories. For example, as current position moves from the location of cache 1 to cache 2, place outputs  
192 discretely jump from one cache location to the other, corresponding to correct selection of the nearest cache location.  
193 The search radius during recall can thus be flexibly adjusted according to task demands, allowing the trade-off between  
194 pattern completion and pattern separation to be dynamically regulated by simple scaling of a network input.

195 We next systematically quantified model performance on these tasks. For these analyses, we binarized the  
196 seed output as being above or below a threshold (Figure S3AB). When caches are sufficiently spaced, memory recall  
197 is near perfect (Figure S3AB). This led us to evaluate the resolution of the model’s memory as caches become more  
198 closely spaced. We decreased the distance between cache 1 and 2 to identify the minimum distance where caches are  
199 separable, i.e. where the model correctly indicates the absence of a cache at a midpoint between caches 1 and 2. Figure  
200 4E shows this correct reject rate as a function of the distance from each cache and the seed input strength. With low  
201 seed input (e.g.  $s = 0$ ), the correct reject rate is high when the current location is one site distance away from caches  
202 1 and 2. In other words, if a cache is made at site 1 and site 3, our model recognizes that site 2 remains empty. This  
203 precision matches the single-site resolution measured by behavioral experiments in this arena (Applegate and Aronov,  
204 2022). As expected, performance on the Cache Presence task decreases with greater seed input strengths, as these are  
205 suited to searching over a broad spatial range.

206 For the Cache Location task, we measure the probability that the model outputs the location of the nearest  
207 cache. We plot this probability as a function of distance from the current location to the nearest cache (Figure 4F). The  
208 model is able to correctly recall cache locations with almost perfect accuracy when it is near a cache. Performance drops  
209 sharply with distance when the seed input is low, but is substantially recovered by increasing the seed input strength.  
210 Critically, even when the search radius is broad enough to include multiple caches, attractor dynamics encourage  
211 selection of the single closest cache location rather than blending memories. Thus the seed input strength provides  
212 a flexible search radius during the recall process. Low values of  $s$  are more suitable for detecting the presence or  
213 absence of a seed near the current location, while high values of  $s$  are more suitable for finding remote caches. The  
214 complementary demands of the Cache Presence and Cache Location tasks demonstrate the utility of a flexible search  
215 radius within one memory system.

216 We further examined how model hyperparameters affected performance on these tasks. We find that the  
217 plasticity bias  $\beta$  is needed to prevent erroneous memory recall at sites without caches (Figure S3E-H). Without this,  
218 recall specificity is poor and model performance suffers on the Cache Presence task. We also verified that our model is  
219 robust to the order in which caches were made (Figure S3CD). Finally, we extended our model to work with random,  
220 spatially correlated inputs, rather than receiving place cell-like inputs (Figure S4). This shows that our results apply  
221 regardless of the specific format of spatial inputs, which are experimentally undetermined.

## 222 **2.5 Place activity and barcode activity play complementary roles in memory.**

223 We have shown that a barcode-mediated memory system is precise yet allows flexible, content-based retrieval. Below  
224 we identify the specific contributions of place and of barcode activity by ablating either of these components in our  
225 model. To ablate barcodes (“Place Code Only” in Figure 5), we initialize our model without the random recurrent  
226 weights that produce chaotic dynamics. This is akin to running caching dynamics in “visit mode”, i.e.  $r = 0$  in Figure  
227 2. To ablate place activity (“Barcode Only” in Figure 5), we eliminate spatial correlations in the networks inputs. This

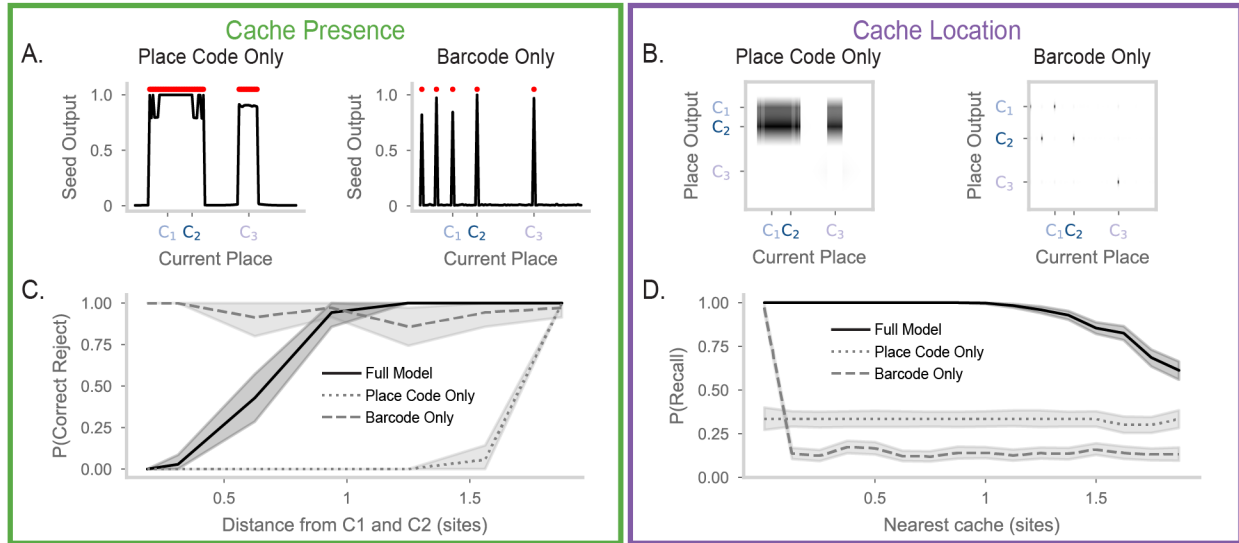


Figure 5: **Ablations reveal complementary roles of place code and barcode activity in memory recall.** **A.** Left, as in Figure 4C, bottom, but for the “Place Code Only” model (barcode-ablated), which has recurrent weights initialized with  $\mu = 0, \sigma = 0$ . Right, same, but for the “Barcode Only” model (place-ablated). The barcode only model is the same as the full model, but place inputs are uncorrelated for nearby locations. **B.** Left, as in Figure 4D, bottom, but for the place code only model. Right, the same but for the barcode only model (for visual clarity, the matrix is downsampled to remove zero-value rows). The place code only model has similar outputs for recall from all current locations. The barcode only model has no place output for recall from most locations. **C.** As in Figure 4E, but showing the full model (solid line), the place code only model (dotted line), and the barcode only model (dashed line). For all models,  $s = 0$ . The place code only model is unable to discriminate between nearby caches. **D.** As in Figure 4F, with lines as in (C). For all models,  $s = 0.4$ . The barcode only model recalls successfully only when the current location contains a cache. Only the full model reliably recalls remote cache locations.

228 is akin to having place fields with extremely narrow precision, rather than a spatially smooth place code. We test both  
 229 ablated models on the three-cache tasks from above and compare their performance to our full model.

230 The Place Code Only model directly binds memory contents of place and seed. This causes cache memories  
 231 for nearby locations, where the place code is correlated, to interfere with each other. Interference is clearly visible in  
 232 the performance on the Cache Presence task (Figure 5A, left). The seed output of the place code only network is high  
 233 across a wide area including caches 1 and 2 and the empty locations between them. Indeed this network is unable to  
 234 identify the absence of a cache at locations between caches 1 and 2, even with a substantial distance between them  
 235 (Figure 5C). Furthermore, the memories for caches 1 and 2 sometimes appears to suppress memory for a distant cache  
 236 3. Further evidence of interference is apparent in the Cache Location task, where the network merges caches 1 and  
 237 2, and entirely fails to signal the cache at location 3 (Figure 5B, left). This network has a low true negative rate, and  
 238 often a single cache dominates the output (Figure S5A-D). Accordingly, the network is able to signal the location of a  
 239 cache, but this location is often not the nearest cache (Figure 5D). Intuitively, without barcodes the network is unable to  
 240 distinguish individual memories at nearby spatial locations. Without this barcode-mediated competition, it forms a  
 241 single agglomerated memory that is inflexibly recalled.

242 If correlations in inputs cause memory interference, why not do away with them entirely? The Barcode Only  
 243 model shows that this is not a good option. This model performs well on the Cache Presence task (Figure 5A, right,

244 Figure S5E-G), correctly identifying the presence of all three caches, and the absence of caches in other locations  
245 (Figure 5C). However, the Barcode Only model fails on the Cache Location task. The model is unable to recall place  
246 fields that are not precisely at its current location (Figure 5B,D). With greater seed input, the model can sometimes  
247 recall memories at remote locations, but these are selected randomly with no preference for nearby caches (Figure 5D,  
248 Figure S5H). Intuitively, the model cannot distinguish nearby and distant caches because it lacks input correlations,  
249 which establish the measure of proximity.

250 In summary, place and barcode activity play complementary roles in our model. Barcode activity functions  
251 like an index for individual memories. This function supports discriminability of memories even when memory contents  
252 overlap – for example, for two nearby caches with correlated place activity. Barcodes also support selective recall  
253 of individual memories in our model via competitive attractor dynamics. However the discriminability advantage of  
254 barcodes is only useful if they can be reactivated during memory recall. Spatially correlated place inputs (and the  
255 seed input) allow efficient memory retrieval by defining a measure of proximity in memory contents, and support  
256 remote memory recall. The presence of both index and content signals in our model allows all of these functions to be  
257 performed by the same network, and for the trade-offs between them to be adjusted flexibly.

## 258 **2.6 Modulating recurrent strength allows the RNN to incorporate both predictive maps and** 259 **barcode memory.**

260 We have constructed a model of a simple episodic memory, taking inspiration from hippocampal data (Chettih et al.,  
261 2024). However, the hippocampus has also been suggested to support functions beyond episodic memory. An especially  
262 influential line of prior work proposes that the hippocampus plays a role in generating predictive maps, with evidence  
263 from both experiments (including in food-caching birds) (Muller and Kubie, 1989; Mehta et al., 2000; Payne et al.,  
264 2021; Applegate et al., 2023) and theory (Blum and Abbott, 1996; Stachenfeld et al., 2017; Whittington et al., 2020).  
265 This raises the question – is our model consistent with predictive map theories? And if so, how might predictive maps  
266 influence episodic memory recall?

267 Interestingly, prior work has shown that biologically realistic RNNs can generate predictive maps with  
268 structured recurrent weights (Fang et al., 2023). Specifically, if recurrent weights encode the transition statistics of an  
269 animal’s experience, then predictive map-like activity will arise from the RNN dynamics, and can be controlled by  
270 recurrent strength (analogous to the value of  $r$  in equation 3). This prediction via structured recurrent weights invites  
271 comparison to the use of random recurrent weights in our model to generate barcodes. Inspired by this connection,  
272 we considered whether a single model could generate both predictive and barcode activity via recurrent dynamics.  
273 We constructed a hybrid model, in which recurrent weights are a blend of random weights, as above, and structured,  
274 predictive weights as in Fang et al. (2023) (Figure S6AB). We hypothesize that network activity changes from a  
275 predictive to a chaotic regime (supporting barcodes) with increasing recurrent strength, i.e. as we adjust  $r$  in the range  
276  $0 < r < 1$ .

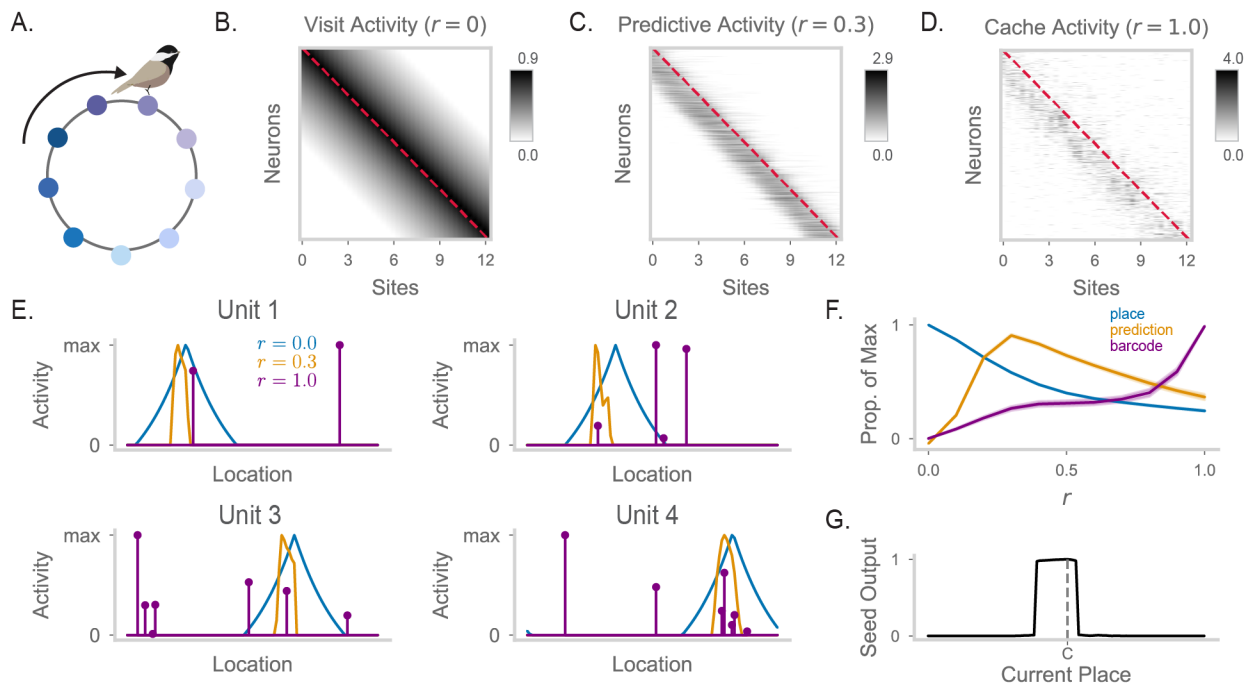


**Figure 6: Predictive coding and barcode generation are performed by the same RNN in different dynamical regimes** **A.** Cartoon of a chickadee in a circular track, running in a consistently clockwise direction. **B.** Heatmap of RNN firing fields when  $r = 0$ , where each row corresponds to the tuning curve of one neuron across all locations. Red dashed line indicates the diagonal. **C.** As in (B), but for  $r = 0.3$ . Here, clockwise movement corresponds to movement from site  $i$  to site  $i + 1$ . Thus predictive activity appears as a shift in RNN activity below the matrix diagonal. **D.** As in (B), but for  $r = 1.0$ . Barcodes appear as random, off-diagonal structure in the activity matrix. **E.** The firing fields of four example units across different recurrent strengths. That is, each unit's row in (B) is in blue, its row in (C) is in orange, and its row in (D) is in purple. Each curve is max-normalized. **F.** Average projection strength of RNN activity onto the place code, predictive code, and barcode vectors. The place code vector is defined as activity with  $r = 0$ . The predictive code vector is defined as the place field of the unit at the next clockwise site, minus the projection onto the place code. The barcode vector is defined as activity with  $r = 1.0$ , minus the projection onto the place code. Each line is max-normalized. **G.** Seed output of the model with predictive weights, given the animal's location on the circular track. Here, there is only one cache, made at the halfway location of the circular track (labeled "C").

277 We use the same circular arena for our simulations, but with the assumption that animal behavior is biased,  
 278 i.e., the animal only moves clockwise (Figure 6A). We visualize population activity at each site, with units sorted  
 279 by their place field. When recurrent strength is at its lowest ( $r = 0$ , Figure 6B) network activity is place-like and  
 280 reflects the current location of the animal provided in its inputs. When recurrent strength is slightly increased ( $r = 0.3$ ,  
 281 Figure 6C), the network exhibits predictive activity. That is, neural activity of recurrent units is shifted to reflect an  
 282 expected future position, relative to the current spatial position encoded in inputs. This is consistent with observations  
 283 from experimental data collected from hippocampus of animals with biased movements in a linear track (Wilson and  
 284 McNaughton, 1993; Mehta et al., 1997, 2000; Lisman and Redish, 2009). Finally, when recurrent strength is maximal  
 285 ( $r = 1.0$ , Figure 6D) we observe barcodes, i.e. sparse activity at random positions relative to inputs. We plot spatial  
 286 tuning curves of a few example RNN units under low, intermediate, and high recurrent strengths (Figure 6E, S6C).  
 287 Individual units can display typical place fields (blue), skewed predictive place fields (orange), and barcode activity  
 288 (purple).



289 These results suggest that the structured and random components of recurrent connectivity can act somewhat  
290 independently of each other, with their relative contributions determined by recurrent strength. We quantify this by  
291 measuring the magnitude of the projection of population activity onto the place code, the predictive code, and barcodes  
292 as a function of recurrent strength (Figure 6F). At the lowest recurrent strength ( $r = 0$ ), the population activity is  
293 solely concentrated on the place code. As recurrent strength is increased, place coding decreases and predictive activity  
294 increases with a peak around  $r = 0.4$ . Beyond this, both place and predictive activity decrease as barcode activity rises  
295 to a peak when  $r = 1.0$ .

296 Finally, we explore the functional implications of including predictive maps into our memory model. We first  
297 verify that model performance in the previous three-cache tasks is not disrupted by including predictive weights in the  
298 model (Figure S7). We then examine memory recall of a single cache for a predictive model, assuming a clockwise  
299 behavioral bias (Figure 6G). The model exhibits a profound skew: the cache is recalled much earlier on the path leading  
300 up to the cache location, at further distance from the cache than on the path after the cache location. This indicates that  
301 knowledge of the environment and prior experience, as reflected in predictive place activity, can shape memory recall in  
302 our model.

### 303 **3 Discussion**

304 We have proposed a biologically realistic model for a simple form of episodic memory using barcodes. Our work is  
305 related to previous auto-associative memory models of the hippocampus such as Hopfield networks (Gardner-Medwin,  
306 1976; McNaughton and Morris, 1987; Marr et al., 1991; Alvarez and Squire, 1994; Tsodyks, 1999), but diverges in  
307 a few critical areas. Building on ideas from hippocampal indexing theory (Teyler and DiScenna, 1986; Teyler and  
308 Rudy, 2007), and following the discovery of barcodes (Chettih et al., 2024), we show how recurrent computation can  
309 implement memory indexing. Our model is further noteworthy in randomly intermixing representations of memory  
310 index and memory content in the activity of single neurons, matching experimental findings. This intermixing implies  
311 that single neurons cannot be definitively identified as “place cells” or “barcode cells”, despite clear differentiation  
312 between the place code and the barcode at the population level. A further innovation of our model is the ability to  
313 control the trade-off between pattern completion and pattern separation during memory recall, by simply turning up or  
314 down the strength of a memory content input (“search strength” in Figure 4). In this work we considered only place  
315 and a single “seed” input, but it is straightforward to generalize this to naturalistic cases where different food types are  
316 stored, or to memory contents beyond cached food. In principle, our approach would allow independent control of  
317 search strength for each potential element of memory content.

318 To generate barcodes during caching and retrieval without affecting place activity during visits, our model  
319 changes recurrent strength in an RNN between different behaviors. A major question is how the brain could implement  
320 such gain changes in recurrence. One possible mechanism is a change in recurrent inhibition, which is consistent with  
321 dramatic changes in the activity of inhibitory neurons observed during caching (Chettih et al., 2024). Neuromodulators

322 like acetylcholine have been shown to bidirectionally modulate different inhibitory neuron subtypes (Xiang et al., 1998;  
323 Lovett-Barron, 2014), and proposed to control the recurrent gain of hippocampal processing (Hasselmo, 1999, 2006).  
324 However, our model uses generic RNN units, and it is unclear precisely how units in the model should be mapped to  
325 real excitatory and inhibitory hippocampal neurons in the brain. Our model predicts a state change in hippocampal  
326 activity during memory formation and recall, allowing recurrent computation to generate or reactivate memory barcodes.  
327 Detailed modeling of realistic E-I networks is needed to further clarify its specific biological implementation.

328 Alternatively, other mechanisms may be involved in generating barcodes. We demonstrated that conventional  
329 feed-forward sparsification (Babadi and Sompolinsky, 2014; Xie et al., 2023) was highly inefficient, but more specialized  
330 computations may improve this (Földiák, 1990; Olshausen and Field, 1996; Sacouto and Wichert, 2023; Muscinelli  
331 et al., 2023). A separate possibility is that barcodes are generated in a circuit upstream of where memories are stored,  
332 and supplied as inputs to the hippocampal population. We suspect separating barcode generation and memory storage  
333 in separate networks would not fundamentally affect our conclusions.

334 We showed that barcodes allow for precise memory retrieval despite the presence of other correlated memories.  
335 This sharpened memory retrieval is similar to mechanisms used in key-value memory structures that are often embedded  
336 in machine learning architectures (Graves et al., 2014, 2016; Sukhbaatar et al., 2015; Le et al., 2019; Banino et al., 2020).  
337 At their simplest, these key-value memory structures consist of memory slots. Each slot consists of a memory that can  
338 be content-addressed via "keys" such that their stored memory is returned as "values". In machine learning, key-value  
339 memory has been connected to the dot-product attention mechanism used in transformers (Krotov and Hopfield, 2016;  
340 Ramsauer et al., 2020). Interestingly, prior theoretical work has suggested neural implementations for both key-value  
341 memory and attention mechanisms, arguing for their usefulness in neural systems such as long term memory (Kanerva,  
342 1988; Tyulmankov et al., 2021; Bricken and Pehlevan, 2021; Whittington et al., 2021; Kozachkov et al., 2023; Krotov  
343 and Hopfield, 2020). Our work suggests that the hippocampus may use principles similar to those of key-value memory  
344 structures to store episodic memories.

345 Episodic memory is often studied at a behavioral level in humans performing free or cued recall of remembered  
346 word lists (Kahana, 1984; Naim et al., 2020). Temporal context models (TCM) of episodic memory have been highly  
347 successful in accounting for the sequential order effects observed reliably in this experimental setting (Howard and  
348 Kahana, 2002; Howard et al., 2005; Sederberg et al., 2008), and the idea of a "context vector" in TCM is closely related  
349 to use of barcodes as a memory index in our model. However experiments have shown that chickadee cache retrieval  
350 does not exhibit temporal order effects (Applegate and Aronov, 2022), suggesting that caches at different locations are  
351 likely not linked by a temporal context as in TCM. Interestingly, caches at the same location were found to have distinct  
352 but correlated barcodes (Chettih et al., 2024), which could be related to caches sharing a "spatial context" analogous to  
353 TCM. In the present study we did not consider memory for different caches at the same location, since it requires a  
354 mechanism for forgetting or overwriting cache memory following retrieval. Although such "directed forgetting" is  
355 observed in chickadee behavior (Sherry, 1984), there is no definitive solution for Hopfield-like networks, and it is thus  
356 beyond the scope of our current work.

357 Our hippocampal model focused on the implementation of episodic memory. Importantly, the proposed  
358 barcode mechanism is capable of coexisting with other hippocampal functions, such as predictive coding as formalized  
359 by the successor representation (SR) (Stachenfeld et al., 2017). Surprisingly, we found that a hybrid network can switch  
360 between SR-generating and barcode-generating modes of operation by adjusting the gain of recurrent connectivity.  
361 Further work is needed to characterize the general conditions under which barcode and SR functions do or do not  
362 mutually interfere. It is also unclear if these are separate functions of the same circuit, or if they are complementary in  
363 certain scenarios (Schapiro et al., 2017; Barron et al., 2020). For example, we found that the SR could bias barcode-  
364 mediated memory recall. In a complex environment, the Euclidean distance between two points may not correspond to  
365 its proximity in a practical sense, which the SR better captures. In this case, experience-dependent biases in memory  
366 recall can be functionally advantageous (Dasgupta and Gershman, 2021) and would be consistent with behavioral  
367 results (Kahana, 1996; Talmi and Moscovitch, 2004).

## 368 Acknowledgments

369 We thank Kim Stachenfeld, Ashok Litwin-Kumar, and members of the Aronov, Stachenfeld, and Abbott labs for  
370 feedback on this work. This research was supported by the Gatsby Charitable Foundation and the Kavli Foundation and  
371 by NSF award DBI-1707398, NIH Director’s New Innovator Award (DP2-AG071918), NIH Pathway to Independence  
372 Award (SC, 1K99NS136846), NSF GRFP (CF), and DOE CSGF (JL, DE–SC0020347).

## 373 Contributions

374 All authors contributed to conceptualization of this project. CF, JL, and SC designed the network and experiments. CF  
375 and JL performed formal analysis, with supervision by SC, DA and LA. CF, SC and DA prepared the manuscript with  
376 feedback from all authors.

## 377 Methods

### 378 Caching Task

379 We simulate a caching task in a circular track, similar to Chettih et al. (2024). The track consists of  $N_s$  connected states.  
380 The goal of this task is to test how well an agent equipped with a memory model can precisely recall the locations  
381 where a cache (or memory) has been stored. Specifically, for each simulation we first choose a set of states  $C$  that will  
382 be the location where caches are made. For each state  $c \in C$  we assume the agent is currently at state  $c$  and allow the  
383 model to store a memory at that state. We then simulate what the output of the model is if the agent is at any of the  
384 other  $N_s$  states. We continue this procedure for the remaining states in the list.

385 In the three-cache task,  $C = \{0, m, N_s * 0.7\}$ . We sweep over different values of  $0 < m < N_s * 0.7$  to test the  
 386 effects of site spacing. In the main figures, these three caches are made in increasing order of their location. However,  
 387 we also randomly shuffle the order of caching in a supplementary figure (Figure S3CD) and do not find any effects on  
 388 model performance.

## 389 Barcode model

### 390 Architecture

391 Place inputs into the model arrive from an input layer  $\vec{p} \in \mathcal{R}^{N_p}$ . The input layer feeds into a recurrent neural network  
 392 with activity  $\vec{x} \in \mathcal{R}^{N_x}$ , where  $N_x = N_p$ . Place input units connect to recurrent units with one-to-one connections  
 393 (that is, the weight matrix  $J_{xi}$  from the place input layer to the recurrent network is the size  $N_x$  identity matrix).  
 394 Recurrent weights are encoded in the matrix  $J \in \mathcal{R}^{N_x \times N_x}$ . At initialization,  $J \sim \mathcal{N}(\frac{\mu}{N_x}, \frac{\sigma^2}{N_x})$  where  $\mu, \sigma$  are tunable  
 395 hyperparameters controlling the mean and standard deviation of the distribution.

396 The input representing seeds arrives from a single unit  $s$ . The connections from  $s$  to recurrent units  $\vec{x}$  are  
 397 encoded in the vector  $\vec{j}_{sx} \in \mathcal{R}^{N_x}$ . Each value of  $\vec{j}_{sx}$  is sampled from the standard normal distribution.

### 398 Recurrent dynamics

Recurrent dynamics are run over  $T$  timesteps. Let  $\vec{v}_t$  be the preactivations of the recurrent population at time  $t$  and  $\vec{x}_t$   
 be the activations of the recurrent population at time  $t$ . That is,  $\vec{x}_t = ReLU(\vec{v}_t)$ . At  $t = 0$ ,  $\vec{x}_0 = \vec{v}_0 = 0$ . The recurrent  
 dynamics are defined over  $\vec{v}$ :

$$\frac{d\vec{v}}{dt} = \left( -\frac{\alpha}{N_x} \sum \vec{x} \right) \vec{v} + rJ\vec{x} + \vec{p} + s\vec{j}_{sx}$$

399 where  $r \in \{0, 1\}$  is a modulatory factor that controls whether the network operates with recurrent dynamics or is purely  
 400 feedforward driven. The first term in the equation corresponds to a voltage leak term where the leak at each neuron is  
 401 proportional to global population activity. This effectively implements a form of divisive normalization, and helps keep  
 402 network activity stable even as weights are updated during the caching task. The second term in the equation represents  
 403 recurrent inputs, while the last two terms represent feedforward inputs into the network.

### 404 Input structure and timing

405 Place is encoded in  $\vec{p}$  such that, at location  $k$ , each input neuron  $l$  has activity  $p_l = e^{-\frac{d}{v}}$  where  $d$  is the shortest distance  
 406 between  $k$  and  $l$  as a percentage of the circular arena size. We consider 100 evenly sampled states in this state space.  
 407 Seed input  $s$  may be any nonnegative scalar value.

- 408 • Place mode: Input  $\vec{p}$  is active over all  $T$  timesteps. Recurrence is turned off ( $r = 0$ ), as is the seed input  
 409 ( $s = 0$ ).
- 410 • Caching mode: Input  $\vec{p}$  is active over all  $T$  timesteps and input  $s$  is active over timesteps  $[T - t_s, T]$  with  
 411 strength  $\lambda$ . Recurrence is on ( $r = 1$ ).

412 • Recall mode: Input  $\vec{p}$  and input  $s$  are both active over all  $T$  timesteps. Recurrence is on ( $r = 1$ ). The value of  
413  $s$  is flexibly modulated to adjust the search strength ( $s \geq 0$ ).

#### 414 Update rule

Let  $\vec{x}$  be the activations of the recurrent network at the end of recurrent dynamics (in our case, at time  $T$ ). At each cache event the update rule carried out is

$$\Delta J = \frac{\eta}{N_x} (\vec{x}\vec{x}^\top + \beta\vec{x}\mathbf{1}^\top)$$

where  $\eta$  controls the learning rate. The weight update contains a Hebbian update through  $\vec{x}\vec{x}^\top$  and an inhibitory update through  $\beta\vec{x}\mathbf{1}^\top$ , where  $\beta$  is a negative scalar. This inhibitory term causes the connections between neurons which are not co-active during caching to weaken. The update rule can also be stated in terms of the synapse  $j \rightarrow i$ :

$$\Delta J_{ij} \sim x_i x_j + \beta x_i$$

415 This is the form shown in equation 4.

#### 416 Network readout

417 To detect cache presence, we define a seed output signal. The output  $y_s$  is read out from the recurrent network activity  
418 through weights  $\vec{j}_{sx}$ . At initialization,  $\vec{j}_{sx} = 0$ . Every time a cache is made, the following update rule is run:  $\Delta\vec{j}_{sx} = \vec{x}$ .  
419 Thus, seed output is read out as  $y_s = \vec{j}_{sx}^\top \vec{x}$ .

420 To recall cache location, we define a place field readout layer. The output  $\vec{y}_p \in \mathcal{R}^{N_p}$  is read out from the  
421 recurrent network through weights  $J_{yx} \in \mathcal{R}^{N_i \times N_x}$ . At initialization,  $J_{yx} = 0$ . Every time a cache is made, the  
422 following update rule is run:  $\Delta J_{yx} = \vec{p}\vec{x}^\top$ . Thus, recalled cache locations are read out as  $\vec{y}_p = J_{yx}\vec{x}$ .

#### 423 Ablations

424 To construct a place code only model, we ablate barcode generation by setting  $J = 0$  at initialization. To construct a  
425 barcode only model, we ablate the presence of place-correlations in the input by setting the place input spatial scale  
426 parameter  $\nu$  to a very small value  $10^{-3}$  in the place encoding equation.

#### 427 Defining site distance in our simulation

428 To allow comparisons to data in [Chettih et al. \(2024\)](#), we first determine the number of states in our simulation that's  
429 equivalent to the distance between adjacent cache sites in [Chettih et al. \(2024\)](#). To do so, we note that the spatial  
430 correlation between population activity at two adjacent cache sites is around 0.75 (when spatial correlation profile is  
431 normalized to  $[0, 1]$ ). We identify the number of states in our simulation such that the normalized correlation between  
432 visit activity is also around 0.75. We find that this is around 8 states. Thus, we define 8 states in our simulation as  
433 equivalent to the distance between adjacent cache sites.

## 434 **Simulating and visualizing spikes**

435 We simulate Poisson spikes from our rate network in Figure 2HJ. Specifically, for a unit with rate  $r$ , we draw spikes  
436 from a Poisson distribution with mean and variance  $r + K$ . We set  $K = 0.2$  to visually match observations from data.

## 437 **Spatial correlation of RNN activity at different sites**

438 To calculate correlation values as in Figure 3D, we average over the correlations across multiple samples of Poisson-  
439 generated population spikes. Specifically, for RNN activity  $\vec{r}_i$  at location  $i$ , we first generate a sample vector of spikes  
440  $\vec{s}_i \sim \text{Poisson}(k\vec{r}_i)$ . We choose  $k$  to be 0.2 to match experimental spatial correlation profiles in the “visit-visit” condition.  
441 To get the correlation of population activity at locations  $i, j$ , we calculate the population Pearson correlation coefficient  
442 between  $\vec{s}_i$  and  $\vec{s}_j$ . To generate Figure 3D, we collect correlation values between sites with caches in an experiment  
443 where 5 caches are made in randomly chosen site locations. All values are normalized by the “visit-visit” correlation  
444 value at a site distance of 0. This is repeated over 20 random seeds.

## 445 **Barcode model with predictive map**

446 The barcode model with prediction differs from the default model in the initialized weight matrix. Specifically,  
447 the weight matrix  $J = B + M$ , where  $B$  is the random Gaussian matrix of the default model.  $M$  is a successor  
448 representation-like matrix (Stachenfeld et al., 2017) defined as

$$M = \rho \left( \sum_{d=0}^D \gamma^d T^d \right) + \delta$$

449 where  $T$  is the transition probability matrix and  $\gamma = 0.99$  is a temporal discount factor. We also add a scaling factor  
450  $\rho = 0.075$  and an inhibitory offset  $\delta = -0.015$ .  $M$  is a 5000-dimensional square matrix, and we truncate the summation  
451 at  $D = 300$  steps.  $T$  is defined as

$$T_{ij} = \begin{cases} 1, & \text{if } j = i + 1 \\ 0, & \text{otherwise} \end{cases}$$

## 452 **Alternative model: feedforward barcode generation**

We will construct a feedforward model to generate sparse, decorrelated barcodes (Figure S2A). Place inputs to the  
model are fed through a hidden expansion layer before being compressed again by an output layer to generate the  
barcode. We first define these layers via the random matrices  $W_h \in \mathcal{R}^{M, N_p}$  and  $W_o \in \mathcal{R}^{N_x, M}$  where  $W_h \sim \mathcal{N}(0, \frac{1}{N_p})$   
and  $W_o \sim \mathcal{N}(0, \frac{1}{M})$ . We make the hidden layer very large:  $M = 20000$ . The activity of the model in the hidden layer  
is described as:

$$\vec{x}_h = \text{ReLU}(W_h \vec{p} - C_\theta)$$



453 where  $C_\theta$  is a constant chosen such that the proportion of units in  $\vec{x}_h$  that are active is  $\theta$ . In other words,  $\theta$  is a  
 454 hyperparameter of the model that sets how sparse the hidden layer activity is.

The hidden layer activity is then passed through the output weights to form the barcode activity generated by the feedforward model:

$$\vec{x} = \text{ReLU}(W_o \vec{x}_h - C)$$

455 where  $C$  is a constant chosen such that the sparsity of  $\vec{x}$  matches the sparsity of barcodes generated in the default RNN  
 456 barcode model.

### 457 **Alternative model: place encoding with Gaussian input weights**

458 We simulate a version of the model with more realistic and complex place inputs. We generated the input currents to the  
 459 RNN units according to a 0-mean multivariate Gaussian process. The statistics of the Gaussian process are chosen  
 460 such that the covariance of the inputs to RNN unit  $i$  and unit  $j$  is an exponentially decaying function of their minimum  
 461 spatial distance  $d$  around the circular arena:  $\Sigma_{i,j} = e^{-\frac{d}{0.4}}$ . All other details of this alternative model is the same as in  
 462 the default.

### 463 **Code**

464 Code is publicly available on <https://github.com/chingf/barcodes>.

### 465 **Parameter values**

Hyperparameter		Symbol	Value
Place Inputs	Spatial scale parameter	$\nu$	0.2
Dimensionality	Number of place input neurons	$N_i$	5000
	Number of recurrent network neurons	$N_x$	5000
	Number of output neurons	$N_y$	5000
	Number of states	$N_s$	100
RNN weight matrix	Scale of RNN initial weight mean	$\mu$	-40
	Scale of RNN initial weight standard deviation	$\sigma$	7
RNN dynamics	Dynamics integration step	$\Delta t$	0.1
	Dynamics divisive normalization strength	$\alpha$	20
	Length of recurrent dynamics	$T$	100
	Length of seed input in caching mode	$t_s$	5
Learning parameters	Strength of seed input during caching	$\lambda$	3.0
	Update learning rate	$\mu$	40
	Update rule inhibition bias	$\beta$	-0.35
Analysis parameters	Readout threshold of seed output	$\kappa$	0.5

## 466 **References**

- 467 Alvarez, P. and L. R. Squire (1994). Memory consolidation and the medial temporal lobe: a simple network model.  
468 *Proceedings of the national academy of sciences* 91(15), 7041–7045.
- 469 Applegate, M. C. and D. Aronov (2022). Flexible use of memory by food-caching birds. *Elife* 11, e70600.
- 470 Applegate, M. C., K. S. Gutnichenko, E. L. Mackevicius, and D. Aronov (2023). An entorhinal-like region in  
471 food-caching birds. *Current Biology* 33(12), 2465–2477.
- 472 Babadi, B. and H. Sompolinsky (2014). Sparseness and expansion in sensory representations. *Neuron* 83(5), 1213–1226.
- 473 Banino, A., A. P. Badia, R. Köster, M. J. Chadwick, V. Zambaldi, D. Hassabis, C. Barry, M. Botvinick, D. Kumaran,  
474 and C. Blundell (2020). Memo: A deep network for flexible combination of episodic memories. *arXiv preprint*  
475 *arXiv:2001.10913*.
- 476 Barron, H. C., R. Auksztulewicz, and K. Friston (2020). Prediction and memory: A predictive coding account. *Progress*  
477 *in neurobiology* 192, 101821.
- 478 Blum, K. and L. Abbott (1996). A model of spatial map formation in the hippocampus of the rat. *Neural Computa-*  
479 *tion* 8(1), 85–93.
- 480 Bricken, T. and C. Pehlevan (2021). Attention approximates sparse distributed memory. *Advances in Neural Information*  
481 *Processing Systems* 34, 15301–15315.
- 482 Chetih, S. N., E. L. Mackevicius, S. Hale, and D. Aronov (2024). Barcoding of episodic memories in the hippocampus  
483 of a food-caching bird. *Cell* 187(8), 1922–1935.
- 484 Clayton, N. S. and A. Dickinson (1998). Episodic-like memory during cache recovery by scrub jays. *Nature* 395(6699),  
485 272–274.
- 486 Dasgupta, I. and S. J. Gershman (2021). Memory as a computational resource. *Trends in cognitive sciences* 25(3),  
487 240–251.
- 488 Fang, C., D. Aronov, L. Abbott, and E. L. Mackevicius (2023). Neural learning rules for generating flexible predictions  
489 and computing the successor representation. *elife* 12, e80680.
- 490 Földiak, P. (1990). Forming sparse representations by local anti-hebbian learning. *Biological cybernetics* 64(2),  
491 165–170.
- 492 Gardner-Medwin, A. (1976). The recall of events through the learning of associations between their parts. *Proceedings*  
493 *of the Royal Society of London. Series B. Biological Sciences* 194(1116), 375–402.
- 494 Graves, A., G. Wayne, and I. Danihelka (2014). Neural turing machines. *arXiv preprint arXiv:1410.5401*.

- 495 Graves, A., G. Wayne, M. Reynolds, T. Harley, I. Danihelka, A. Grabska-Barwińska, S. G. Colmenarejo, E. Grefenstette,  
496 T. Ramalho, J. Agapiou, et al. (2016). Hybrid computing using a neural network with dynamic external memory.  
497 *Nature* 538(7626), 471–476.
- 498 Hasselmo, M. E. (1999). Neuromodulation: acetylcholine and memory consolidation. *Trends in cognitive sciences* 3(9),  
499 351–359.
- 500 Hasselmo, M. E. (2006). The role of acetylcholine in learning and memory. *Current opinion in neurobiology* 16(6),  
501 710–715.
- 502 Hopfield, J. J. (1982). Neural networks and physical systems with emergent collective computational abilities.  
503 *Proceedings of the national academy of sciences* 79(8), 2554–2558.
- 504 Howard, M. W., M. S. Fotedar, A. V. Datey, and M. E. Hasselmo (2005). The temporal context model in spatial  
505 navigation and relational learning: toward a common explanation of medial temporal lobe function across domains.  
506 *Psychological review* 112(1), 75.
- 507 Howard, M. W. and M. J. Kahana (2002). A distributed representation of temporal context. *Journal of mathematical*  
508 *psychology* 46(3), 269–299.
- 509 Kahana, M. J. (1984). Computational models of memory search. *Annual Review of Psychology* 71, 107–138.
- 510 Kahana, M. J. (1996). Associative retrieval processes in free recall. *Memory & cognition* 24(1), 103–109.
- 511 Kanerva, P. (1988). *Sparse distributed memory*. MIT press.
- 512 Kozachkov, L., K. V. Kastanenko, and D. Krotov (2023). Building transformers from neurons and astrocytes. *Proceed-*  
513 *ings of the National Academy of Sciences* 120(34), e2219150120.
- 514 Krotov, D. and J. Hopfield (2020). Large associative memory problem in neurobiology and machine learning. *arXiv*  
515 *preprint arXiv:2008.06996*.
- 516 Krotov, D. and J. J. Hopfield (2016). Dense associative memory for pattern recognition. *Advances in neural information*  
517 *processing systems* 29.
- 518 Le, H., T. Tran, and S. Venkatesh (2019). Neural stored-program memory. *arXiv preprint arXiv:1906.08862*.
- 519 Lisman, J. and A. D. Redish (2009). Prediction, sequences and the hippocampus. *Philosophical Transactions of the*  
520 *Royal Society B: Biological Sciences* 364(1521), 1193–1201.
- 521 Lovett-Barron, M. e. a. (2014). Dendritic inhibition in the hippocampus supports fear learning. *Science* 343(6173),  
522 857–863.
- 523 Marr, D., D. Willshaw, and B. McNaughton (1991). Simple memory: a theory for archicortex. In *From the Retina to*  
524 *the Neocortex*, pp. 59–128. Springer.

- 525 McNaughton, B. L. and R. G. Morris (1987). Hippocampal synaptic enhancement and information storage within a  
526 distributed memory system. *Trends in neurosciences* 10(10), 408–415.
- 527 Mehta, M. R., C. A. Barnes, and B. L. McNaughton (1997). Experience-dependent, asymmetric expansion of  
528 hippocampal place fields. *Proceedings of the National Academy of Sciences* 94(16), 8918–8921.
- 529 Mehta, M. R., M. C. Quirk, and M. A. Wilson (2000). Experience-dependent asymmetric shape of hippocampal  
530 receptive fields. *Neuron* 25(3), 707–715.
- 531 Muller, R. U. and J. L. Kubie (1989). The firing of hippocampal place cells predicts the future position of freely moving  
532 rats. *Journal of Neuroscience* 9(12), 4101–4110.
- 533 Muscinelli, S. P., M. J. Wagner, and A. Litwin-Kumar (2023). Optimal routing to cerebellum-like structures. *Nature*  
534 *neuroscience* 26(9), 1630–1641.
- 535 Naim, M., M. Katkov, S. Romani, and M. Tsodyks (2020). Fundamental law of memory recall. *Physical Review*  
536 *Letters* 124(1), 018101.
- 537 Olshausen, B. A. and D. J. Field (1996). Emergence of simple-cell receptive field properties by learning a sparse code  
538 for natural images. *Nature* 381(6583), 607–609.
- 539 Payne, H. L., G. F. Lynch, and D. Aronov (2021). Neural representations of space in the hippocampus of a food-caching  
540 bird. *Science* 373(6552), 343–348.
- 541 Ramsauer, H., B. Schäfl, J. Lehner, P. Seidl, M. Widrich, T. Adler, L. Gruber, M. Holzleitner, M. Pavlović, G. K. Sandve,  
542 et al. (2020). Hopfield networks is all you need. *arXiv preprint arXiv:2008.02217*.
- 543 Sacouto, L. and A. Wichert (2023). Competitive learning to generate sparse representations for associative memory.  
544 *Neural Networks* 168, 32–43.
- 545 Schapiro, A. C., N. B. Turk-Browne, M. M. Botvinick, and K. A. Norman (2017). Complementary learning systems  
546 within the hippocampus: a neural network modelling approach to reconciling episodic memory with statistical  
547 learning. *Philosophical Transactions of the Royal Society B: Biological Sciences* 372(1711), 20160049.
- 548 Sederberg, P. B., M. W. Howard, and M. J. Kahana (2008). A context-based theory of recency and contiguity in free  
549 recall. *Psychological review* 115(4), 893.
- 550 Sherry, D. (1984). Food storage by black-capped chickadees: Memory for the location and contents of caches. *Animal*  
551 *Behaviour* 32(2), 451–464.
- 552 Sompolinsky, H., A. Crisanti, and H. J. Sommers (1988, Jul). Chaos in random neural networks. *Phys. Rev. Lett.* 61,  
553 259–262.
- 554 Stachenfeld, K., M. Botvinick, and S. Gershman (2017). The hippocampus as a predictive map. *Nature Neuroscience*.

- 555 Sukhbaatar, S., J. Weston, R. Fergus, et al. (2015). End-to-end memory networks. *Advances in neural information*  
556 *processing systems* 28.
- 557 Talmi, D. and M. Moscovitch (2004). Can semantic relatedness explain the enhancement of memory for emotional  
558 words? *Memory & cognition* 32, 742–751.
- 559 Teyler, T. J. and P. DiScenna (1986). The hippocampal memory indexing theory. *Behavioral neuroscience* 100(2), 147.
- 560 Teyler, T. J. and J. W. Rudy (2007). The hippocampal indexing theory and episodic memory: updating the index.  
561 *Hippocampus* 17(12), 1158–1169.
- 562 Tsodyks, M. (1999). Attractor neural network models of spatial maps in hippocampus. *Hippocampus* 9(4), 481–489.
- 563 Tulving, E. et al. (1972). Episodic and semantic memory. *Organization of memory* 1(381-403), 1.
- 564 Tyulmankov, D., C. Fang, A. Vadaparty, and G. R. Yang (2021). Biological learning in key-value memory networks.  
565 *Advances in Neural Information Processing Systems* 34, 22247–22258.
- 566 Whittington, J. C., T. H. Muller, S. Mark, G. Chen, C. Barry, N. Burgess, and T. E. Behrens (2020). The tolman-  
567 eichenbaum machine: unifying space and relational memory through generalization in the hippocampal formation.  
568 *Cell* 183(5), 1249–1263.
- 569 Whittington, J. C., J. Warren, and T. E. Behrens (2021). Relating transformers to models and neural representations of  
570 the hippocampal formation. *arXiv preprint arXiv:2112.04035*.
- 571 Wilson, M. A. and B. L. McNaughton (1993). Dynamics of the hippocampal ensemble code for space. *Sci-*  
572 *ence* 261(5124), 1055–1058.
- 573 Xiang, Z., J. R. Huguenard, and D. A. Prince (1998). Cholinergic switching within neocortical inhibitory networks.  
574 *Science* 281(5379), 985–988.
- 575 Xie, M., S. P. Muscinelli, K. D. Harris, and A. Litwin-Kumar (2023). Task-dependent optimal representations for  
576 cerebellar learning. *Elife* 12, e82914.

577 **A Supplementary Figures**

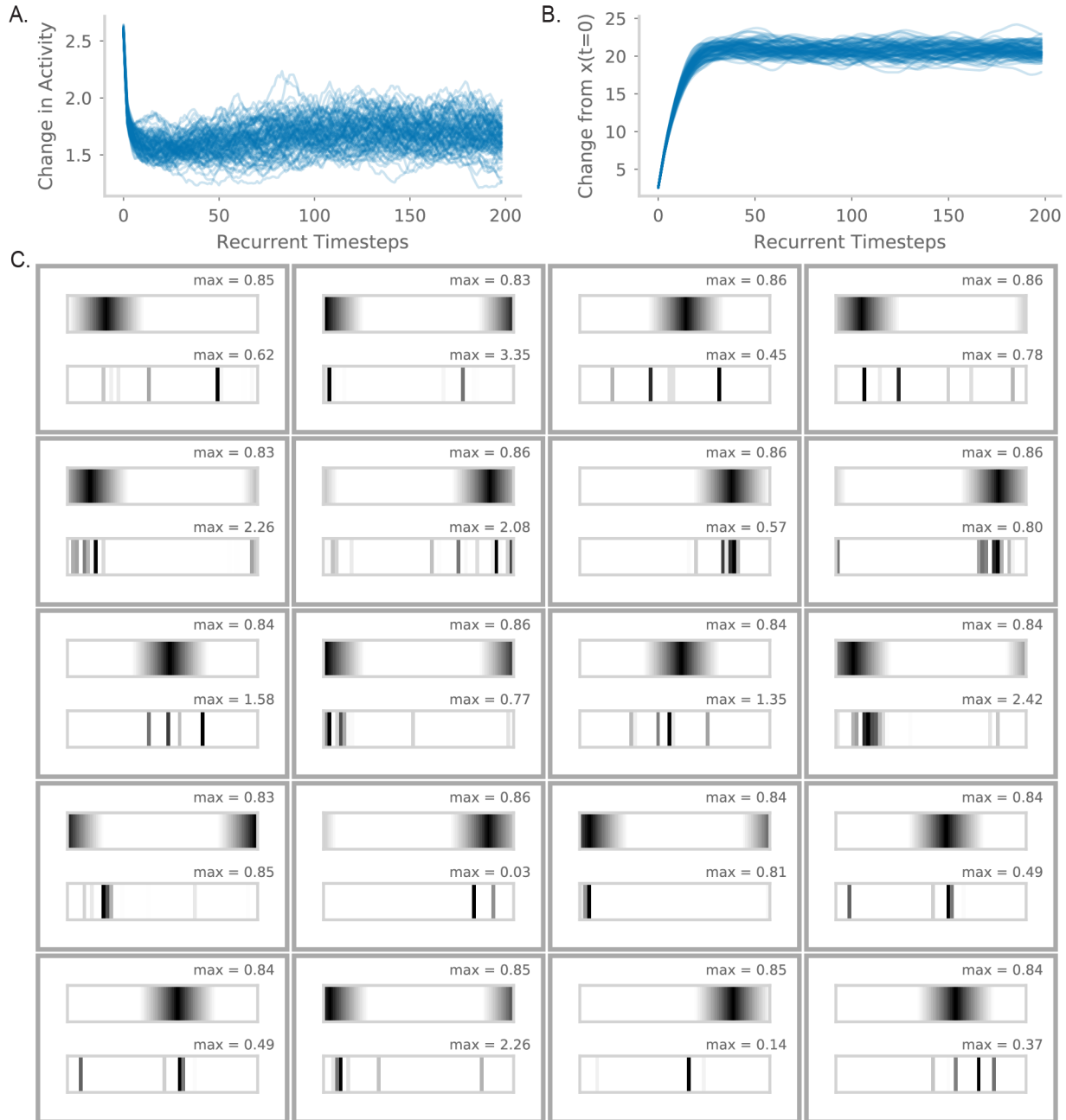


Figure S1: **A.** Difference between RNN activity across each step of recurrent dynamics. Specifically, at recurrent timestep  $t$ , we plot  $|\vec{x}_t - \vec{x}_{t-1}|$ . Each line corresponds to a different random seed and model initialization. **B.** Difference between RNN activity at some step of recurrent dynamics and the initial RNN state. Specifically, at recurrent timestep  $t$ , we plot  $|\vec{x}_t - \vec{x}_0|$ . Each line corresponds to a different random seed and model initialization. **C.** As in Figure 2GI, but for 20 additional randomly sampled units.



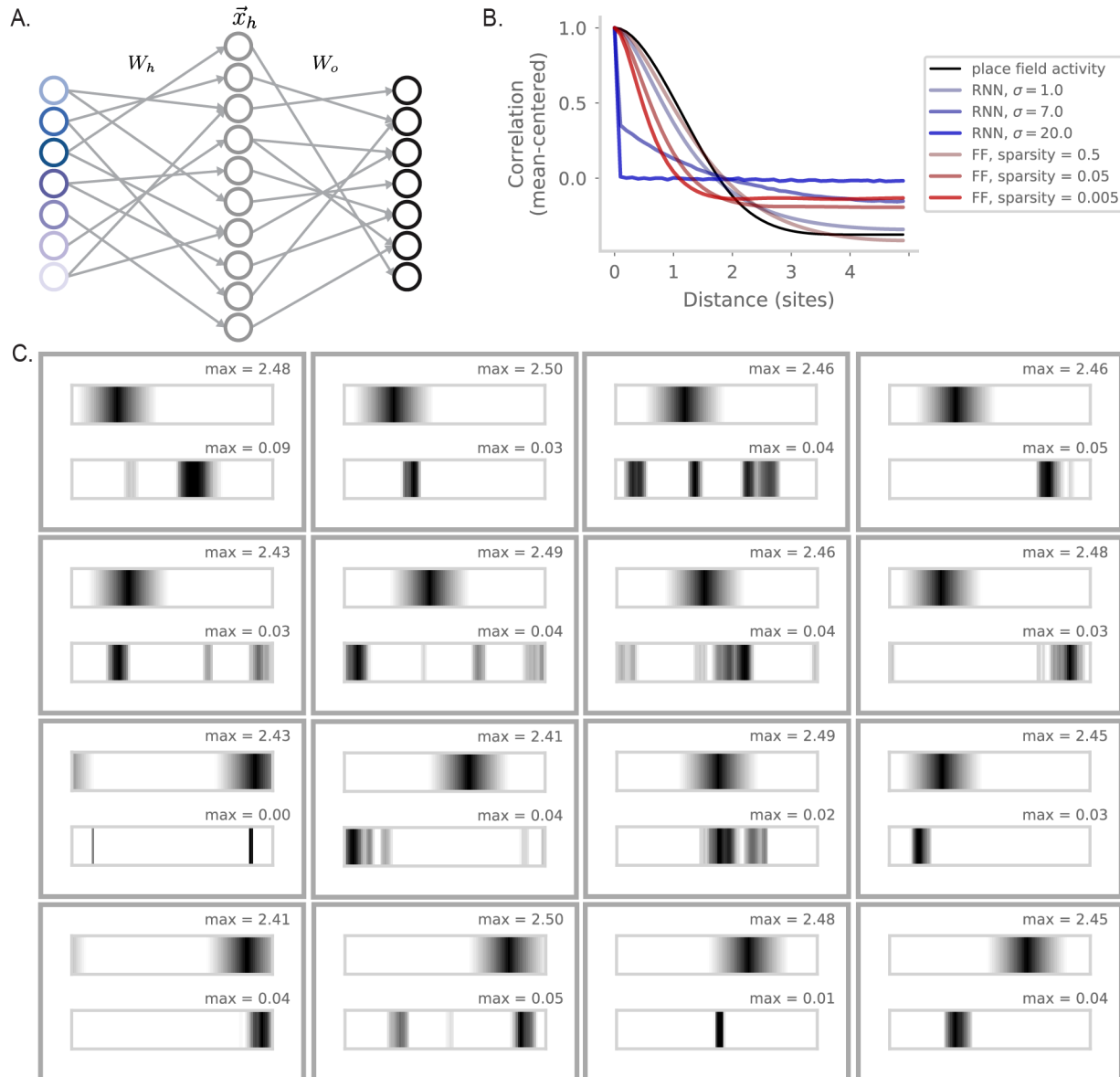


Figure S2: **A.** Diagram of the feedforward model for barcode generation. Place inputs  $\vec{p}$  are passed through an expansion layer  $W_h$  with a nonlinear activation function to get the hidden layer activity  $x_h$ . A subsequent compression layer  $W_o$  with a nonlinear activation function generates the final barcode activity  $x$ . **B.** As in Figure 2B but adding in red the results for the feedforward model as sparsity is varied. **C.** As in Figure 2GI, but for 16 randomly sampled units from the feedforward model.

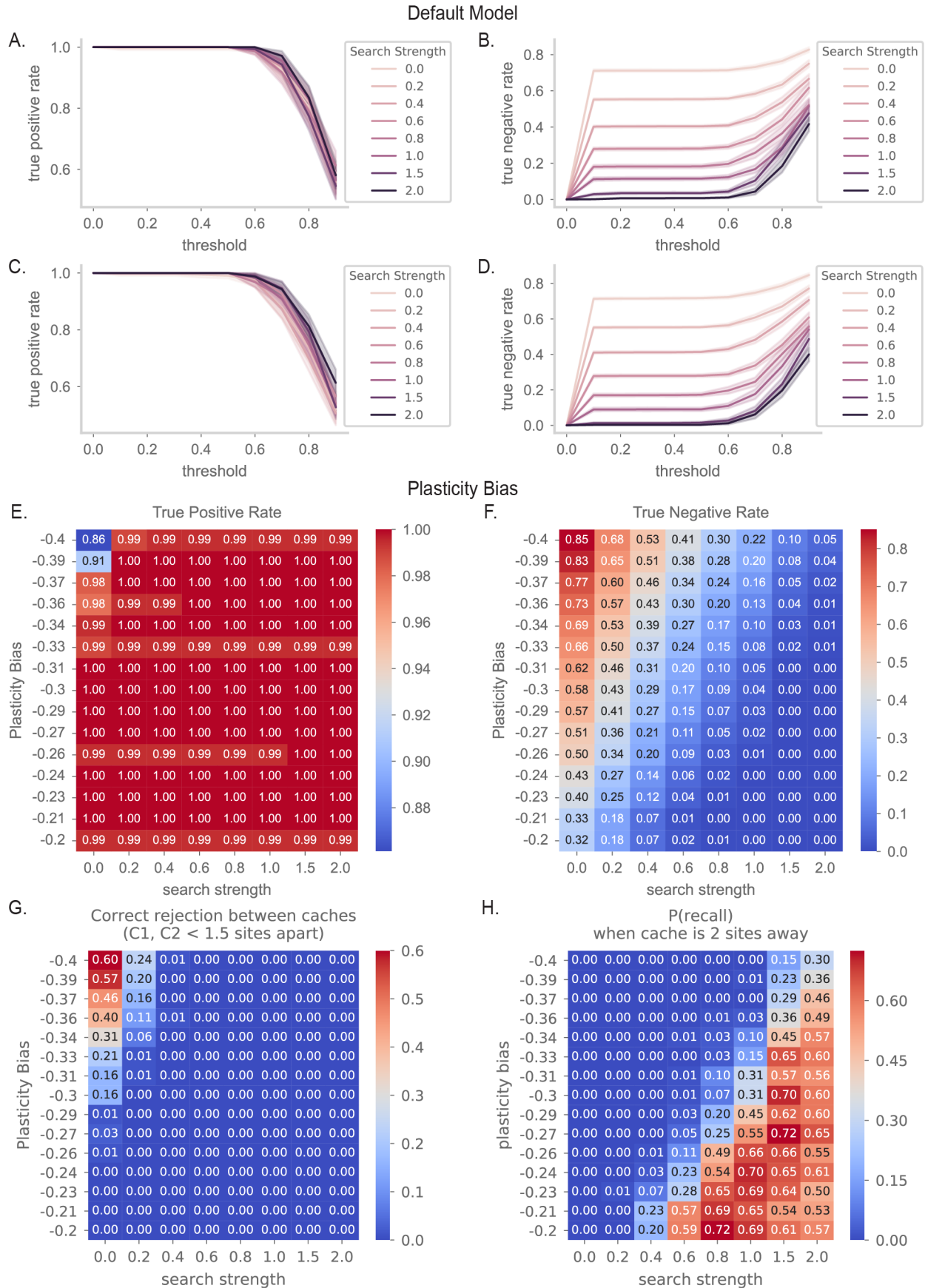


Figure S3: **A.** True positive rate of the seed output in the 3-cache task of Figure 4, as the choice of binarized threshold is varied. The color of each line corresponds to the recall strength  $s$ . Here, caches are all spaced at least two sites apart. **B.** As in (A), but for true negative rate. We will choose a threshold of 0.5 to binarize the seed output. **CD** As in (AB), but the order caches are made is random. **E.** True positive rate of the seed output binarized at 0.5 when plasticity bias  $\beta$  and search strength  $s$  is varied. **F.** As in (E) but for true negative rate. **G.** As in (E) but plotting the correct reject rate at a location between two caches. Here the two caches are 1.5 sites apart or closer. **H.** As in (E) but plotting the probability of recalling the location of the closest cache when the animal is 2 sites away from it.

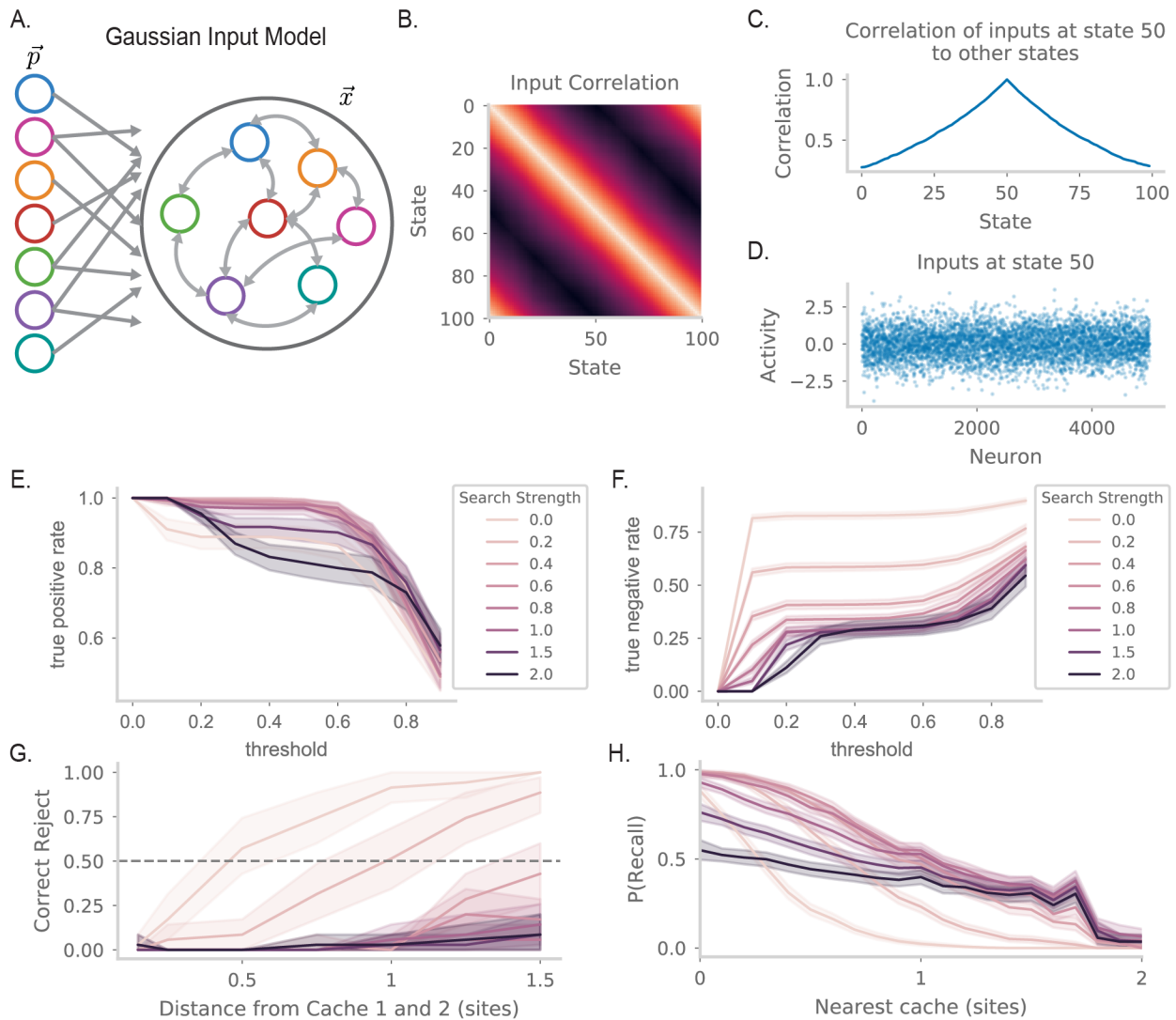


Figure S4: **A.** Diagram showing how place inputs are modified to be more realistic. Place encoding  $\vec{p}$  is now drawn from a 0-mean Gaussian process with place-like covariance structure. This results in a more distributed representation in  $\vec{p}$  over spatial locations. Furthermore,  $J_{xp}$  is now a random Gaussian matrix (instead of the identity matrix). **B.** Correlations between place inputs at different locations, as a function of their distance. **C.** As in Figure S3A, but for the Gaussian model. **D.** As in Figure S3B, but for the Gaussian model. **E.** As in Figure 4E, but for the Gaussian model. **F.** As in Figure 4F, but for the Gaussian model.

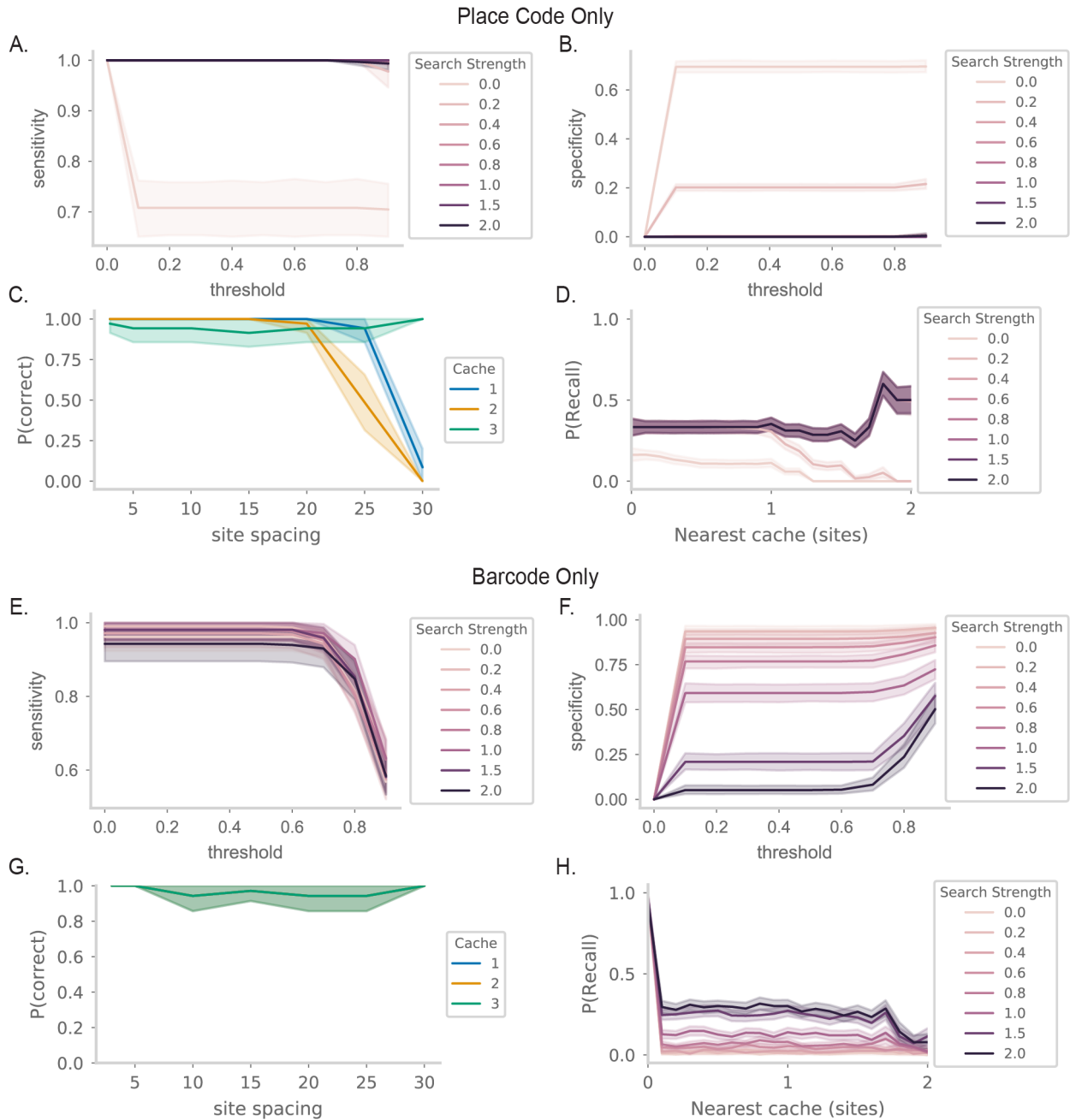


Figure S5: **AB.** As in Figure S3AB, but for the place code only model shown in 5A. **C.** Probability that the  $N$ th cache location is successfully recalled as site spacing is increased in the 3 cache task. Results are shown for the place code only model. **D.** As in Figure 4F, but for the place code only model. **EFGH.** As in (ABCD), but for the barcode only model.

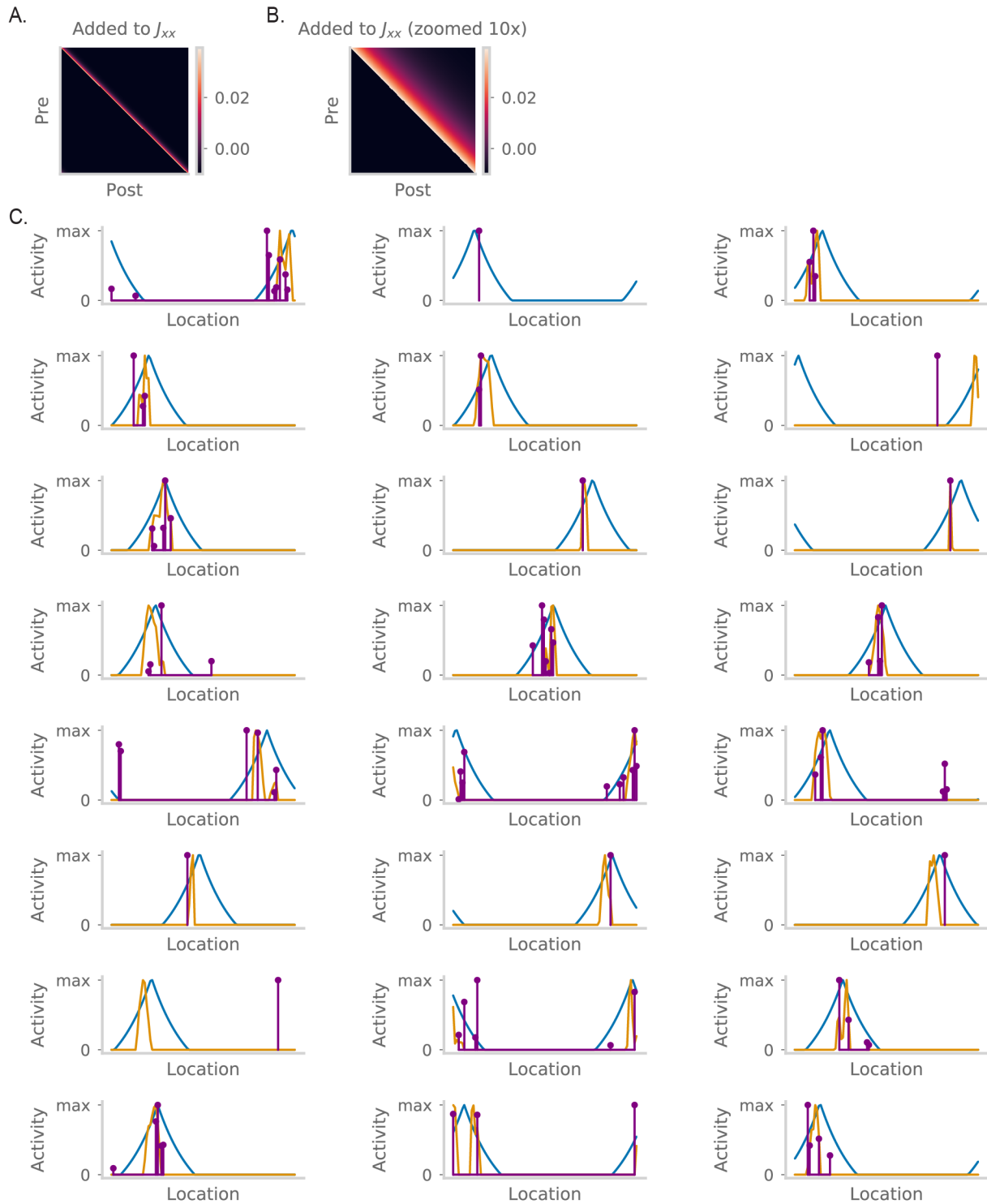


Figure S6: **A.** The predictive weights  $M$  that is added to  $J$ . **B.** As in (A), but zooming in 10x into the matrix for clarity. **C.** As in Figure 6E, but for 24 additional randomly sampled units.

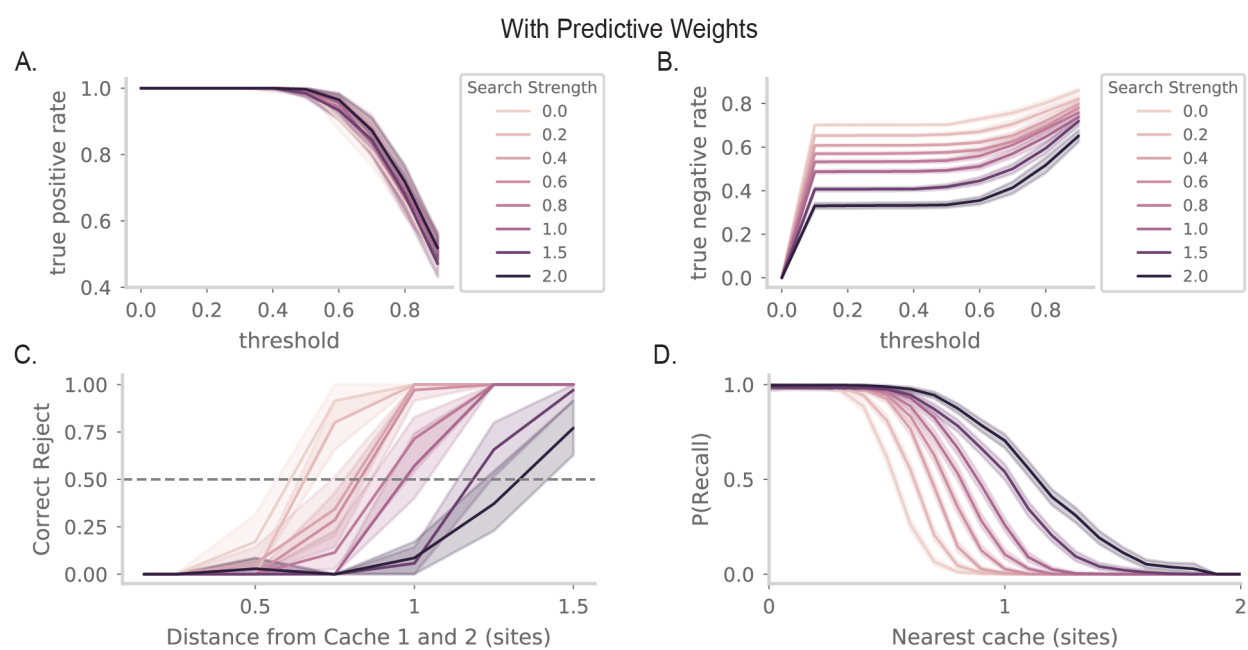


Figure S7: **AB.** As in Figure S3AB, but for the model with predictive weights added in. **CD.** As in Figure 4EF, but the model with predictive weights added in.